ELSEVIER

Heat capacities, order–disorder transitions, and thermodynamic properties of rare-earth orthoferrites and rare-earth iron garnets

S.C. Parida*, S.K. Rakshit, Ziley Singh

Product Development Section, Radiochemistry and Isotope Group, Bhabha Atomic Research Centre, Trombay, Mumbai 400 085, India

Abstract

Rare-earth orthoferrites, $R\mathrm{FeO_3}$, and rare-earth iron garnets (RIGs) $R_3\mathrm{Fe_5O_{12}}$ ($R =$ rare-earth elements) were prepared by citrate–nitrate gel combustion method and characterized by X-ray diffraction method. Isobaric molar heat capacities of these oxides were determined by using differential scanning calorimetry from 130 to 860 K. Order–disorder transition temperatures were determined from the heat capacity measurements. The Néel temperatures (T_N) due to antiferromagentic to paramagnetic transitions in orthoferrites and the Curie temperatures (T_C) due to ferrimagnetic to paramagnetic transitions in garnets were determined from the heat capacity data. Both T_N and T_C systematically decrease with increasing atomic number of R across the series. Lattice, electronic and magnetic contributions to the total heat capacity were calculated. Debye temperatures as a function of absolute temperature were calculated for these compounds. Thermodynamic functions like $C^\mathrm{o}_\mathrm{p,m}$, S^o_m, H^o, G^o, $(H^\mathrm{o}_\mathrm{T} - H^\mathrm{o}_0)$, $(H^\mathrm{o}_\mathrm{T} - H^\mathrm{o}_{298.15\,\mathrm{K}})$, $-(G^\mathrm{o}_\mathrm{T} - H^\mathrm{o}_{298.15\,\mathrm{K}})/T$, $\Delta_\mathrm{f}H^\mathrm{o}_\mathrm{m}$, and $\Delta_\mathrm{f}G^\mathrm{o}_\mathrm{m}$ have been generated for the compounds $R\mathrm{FeO_3(s)}$ and $R_3\mathrm{Fe_5O_{12}(s)}$ based on the experimental data obtained in this study and the available data in the literature.

1. Introduction

Rare-earth iron perovskites (orthoferrites) and rare-earth iron garnets (RIGs) are among some of the important magnetic materials and have extensive applications in materials science and technology. The orthoferrties exhibit a great and bewildering array of magnetic properties. The practical applications of orthoferrites and some of their substituted analogues include high-temperature superconductors, electrode materials in solid oxide fuel cells, electrode materials in magneto-hydrodynamic generators, and materials for sensor technology. In recent years, there has been considerable progress in developing materials that do not exist in nature but can be created artificially by layered deposition of different materials on an atomic or molecular scale to form superlattices. This method has been applied to the formation of ferromagnetic multilayers

from antiferromagnetic (AF) layers of $\mathrm{LaFeO_3}$ and $\mathrm{LaCrO_3}$, $\mathrm{LaFeO_3}$, $\mathrm{LaMnO_3}$, etc. [1–3]. The series of RIGs is probably the most thoroughly investigated one of all ferrites, because of several properties which make the experimental and theoretical studies very rewarding. The RIGs are ferrimagnets and are used in magnetic recording device and show giant magnetorestriction at low temperatures [4]. Similarly, the garnet end members have important applications in laser industry. By substituting various rare-earth ions into the garnet lattice one can study the effect of these ions on the macroscopic properties. Within the rare-earth iron garnets, there are a variety of magnetic interactions, which provide a detailed test for any proposed theoretical model.

Most of the published literature on the physico-chemical properties of these compounds deals with the crystallographic, magnetic, electrical and other physical properties. The thermodynamic properties of these two classes of compounds are reported in several works. Knowledge of thermodynamic properties of these complex oxides is

---
*Corresponding author. Fax: +91 22 2550 5151.
  E-mail address: sureshp@barc.gov.in (S.C. Parida).

essential in selection of materials for suitable technological applications. Thermodynamic data for these oxides are also essential for the computation of phase diagrams for the R–Fe–O systems as well as any higher-order systems involving these basic elements. It is, therefore, important to carry out a systematic study on the thermodynamic properties of these complex oxides from both experimental and theoretical approach. The objective of present study is to investigate the phase transitions in these magnetic oxides, which are expected to be magnetic order–disorder (second order) type transitions. The transition temperatures can be measured accurately from the heat capacity measurements. The heat capacity data can be used to derive the Debye temperatures of these oxides, which is an important parameter to estimate various physical parameters of solids. As a part of systematic studies on these compounds, the heat capacities of these compounds are determined by a differential scanning calorimeter in order to characterize magnetic phase transformations. The heat capacity data are then used with other thermodynamic data to derive various thermodynamic parameters from which thermodynamic tables for some of these compounds were constructed.

1.1. Crystal structure and magnetic ordering in $RFeO_3(s)$

The ternary oxides $RFeO_3(s)$, where R is a rare-earth element, belong to perovskite structure types and are termed orthoferrites to distinguish them from cubic spinel ferrites. The crystal structures of these compounds have been studied in detail by Marezio and Dernier [5]. The structure of an ideal perovskite ABO_3 is shown in Fig. 1. However, the orthoferrites crystallize in an orthorhombically distorted perovskite structure with four molecular unit per unit cell.
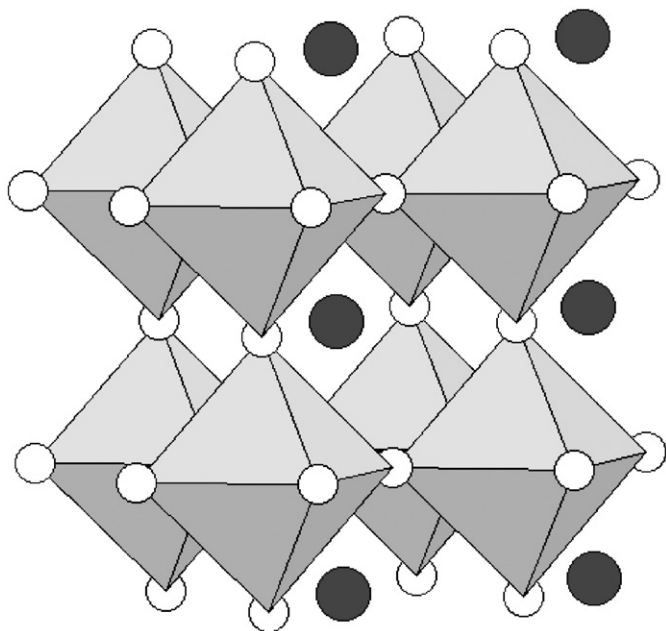
The crystallographic unit cell of a representative compound $NdFeO_3$ is shown in Fig. 2. There is a displacement of Nd atomic position from the ideal position in cubic perovskites. The main distortion is related to the tilts of octahedra around the b and c orthorhombic axes. These tilts are made evident in the Fe–O–Fe bond angles that are lower than the ideal value of 180° in the cubic perovskite. Lower values of these angles lead to higher metal–insulator transition temperatures.

The Fe^{3+} ion is octahedrally co-ordinated by oxygen giving an FeO_6 octahedra. The perovskite can be visualized as corner-linked FeO_6 octahedra favoring a three-dimensional polyhedral network. Rare-earth ions are located in the large cavities formed by these octahedra. The common apex of two adjacent octahedra is the intervening anion that provides the super-exchange bond between two iron ions. Thus, each Fe^{3+} ion is coupled by super-exchange to six Fe^{3+} nearest neighbors, resulting in high Néel temperatures (T_N). The larger the R^{3+}, the super-exchange bond angle approaches 180°. Thus, $LaFeO_3$ has the highest Néel temperature and $LuFeO_3$ the lowest. The crystal data for $NdFeO_3$ [6] are given in Table 1 which is representative of $RFeO_3$.

$RFeO_3$ orthoferrites are magnetically ordered semiconductors reflecting localized $3d$ electrons in the high-spin (HS) state. This feature is revealed in the X-ray and photoelectron spectra of these compounds studied by Lam et al. [7]. Because of the two magnetic ions in the system, $RFeO_3$ generally shows complicated magnetic behavior. The magnetic ordering of the Fe^{3+} ions is essentially AF. However, the symmetry of the magnetic unit cell, which is
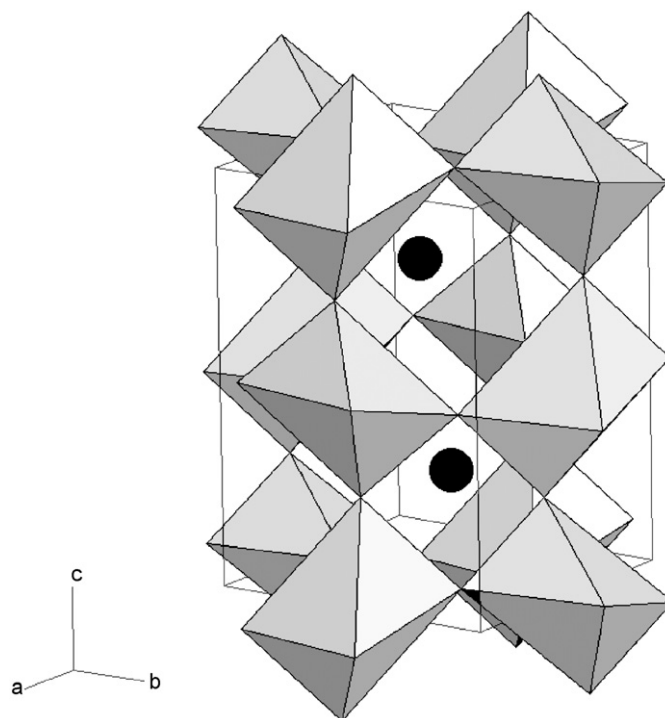

Fig. 1. The structure of an ideal perovskite ABO_3.

Fig. 2. Orthorhombically distorted perovskite structure of $NdFeO_3$.

Table 1
Crystal data on $NdFeO_3$ and $Y_3Fe_5O_{12}$

Compound	NdFeO₃ [6]	Y₃Fe₅O₁₂ [24]
Structure type	Orthoferrite	Garnet
Crystal class	Orthorhombic	Cubic
Space group	P_{bnm}	$Ia3d$
a (Å)	5.4504	12.376
b (Å)	5.5835	12.376
c (Å)	7.6020	12.376
α (deg)	90	90
β (deg)	90	90
γ (deg)	90	90
Z	4	8
ρ_{calc} (g cm^{-3})	6.98	5.17

equal to the crystallographic one, is low, and hence weak ferromagnetism is observed (canted moment). Starting from the paramagnetic state at high temperature, the magnetic moment of Fe^{3+} orders antiferromagnetically around 600–700 K on cooling. Canting of the magnetic moments results in weak ferromagnetism in the Fe^{3+} ordered state as described by Burns [8]. On further cooling, many rare-earth orthoferrites undergo spin-reorientation transitions, where the direction of the net magnetic moment rotates continuously or abruptly from one crystallographic axis to another due to the antisymmetric and anisotropic-symmetric exchange interactions between Fe^{3+} and R^{3+}. In some orthoferrites with antiparallel configurations of Fe^{3+} and R^{3+} moments, vanishing net magnetization occurs at a compensation temperature. Finally, the magnetic moment of R^{3+} orders around or below liquid-helium temperature in some systems. The Fe–Fe coupling is very small because of the perovskite structure. Magnetic couplings of the type Fe–R and R–R are at least two orders of magnitude below the Fe–Fe coupling. The different types of magnetic interactions between Fe^{3+} and R^{3+} follow a hierarchy of Fe–Fe, Fe–R and R–R with decreasing order of strength.

1.2. Spin-reorientation transition in RFeO₃

In many of the orthoferrites, the direction of the easy axis of magnetization is known to change from one crystallographic axis to another as the temperature is raised. These transitions are called spin-reorientation transitions. These transitions are described in two ways:

(1) the easy axis jumps abruptly in a first-order phase transition, possibly exhibiting thermal hysteresis of the transition temperature;
(2) as the temperature is raised the easy axis starts to rotate at one definite temperature T_L and ceases rotation when it reaches a new orientation at another definite temperature T_H. Second-order phase transitions occur at T_L and T_H.

A phenomenological description of the nature of spin-reorientation transitions is described by Horner and Varma [9]. In orthoferrites, the spin-reorientation transition is observed to be of the second type. The net moment of the orthoferrites switches from the c-axis to a-axis.

At very low temperatures of the order of 2–4 K, several of the orthoferrites show a spin ordering which is not primarily a reorientation process, but is characterized by an ordering of the rare-earth ions. The R–R ordering at low temperatures has been confirmed by neutron diffraction work of Koehler et al. [10] for R = Er, Ho and Nd, which confirms that Er^{3+} ions order at 4.3 K, Ho^{3+} at 6.5 K and the Nd^{3+} ions did not order down to 1.25 K. However, Bartolome et al. [11] have observed the Nd^{3+} ordering in NdFeO₃(s) at 1.05 K from specific heat measurements. Specific heat measurements by de Combarieu et al. [12] on TbFeO₃(s) confirm the Tb^{3+} ordering at 3.20 K. Belov et al. [13] found an AF transition near 30 K and an ordering of Dy^{3+} ion near liquid-helium temperature. Gorodetsky et al. [14,15] found the AF transition at 36 K and Dy^{3+} ordering temperature at 3.7 K. Berton and Sharon [16] have carried out specific heat measurements on DyFeO₃(s) from 1.2 to 80 K and found the Dy^{3+} ordering at 3.7 K. Moldover et al. [17] carried out specific heat measurements on YbFeO₃(s) and found out the Yb^{3+} ordering at 4.6 K. Bhattacharjee et al. [18] have observed the Ho^{3+} ordering temperature at 3.3 K from specific heat measurements. Saito et al. [19] have observed the Er^{3+} ordering temperature at 3.60 K from specific heat measurements. No ordering for Tm^{3+} has been observed so far. La^{3+} and Lu^{3+} ions are non-magnetic and do not expect to show magnetic ordering. The magnetic disordering temperature (Néel temperature = T_N) in orthoferrites has been measured by Eibschutz et al. [20] by observing the collapse of the magnetic hyperfine sextet into a singlet in the ^{57}Fe Mössbauer spectra with temperature. Stølen et al. [21] have measured the Néel temperature of LaFeO₃(s) from heat capacity data. Wolf and White [22] have reviewed the magnetic and spectroscopic properties of $RFeO_3$(s). The observed values of T_N and spin-reorientation transition temperatures (T_{SR}) are summarized in Table 2.

1.3. Crystal structure and magnetic ordering in rare-earth iron garnets ($R_3Fe_5O_{12}$)

Magnetic garnets crystallize in the dodecahedral or 12-sided structure related to the mineral garnet. The crystal structure of magnetic garnets were elucidated by Geller and Gilleo [23] with general formula $C3A2D3O12$ whereby A, C and D represent different cations in different structural places. Position C can be occupied by, e.g. Mg^{2+}, Fe^{2+}, Mn^{2+}, Ca^{2+} and Y^{3+}, position A, e.g. with Al^{3+}, Cr^{3+} and Fe^{3+} and position D, e.g. by Al^{3+}, Ga^{3+}, Fe^{3+} and Si^{4+}. For the RIG, C represents R^{3+} whereas A and D both represent Fe^{3+}. The structure of RIG is shown in Fig. 3. The crystal data for $Y_3Fe_5O_{12}$ [24], which is a representative of $R_3Fe_5O_{12}$, are given in Table 1.

Table 2
Values of T_N and spin-reorientation transition temperatures (T_{SR}) of $RFeO_3(s)$ reported in the literature

R	T_{N1}/K [Ref.]	T_{SR} [Ref.]		T_{N2}/K [Ref.]
		T_L/K	T_H/K	
La	740 [20]			
	735 [21]			
Pr	707 [20]			
Nd	687 [20]			
	690 [20]	125	167	1.05 [11]
Sm	674 [20]	>400		
Eu	662 [20]			
Gd	657 [20]			
Tb	647 [20]			3.1 [22]
				3.2 [12]
Dy	645 [20]			3.7 [22]
	645 [20]			
Ho	639 [20]	53	58	6.5 [22]
				3.3 [18]
Er	636 [20]			4.3 [22]
				3.60 [19]
Tm	632 [20]	82	89 [19]	
Yb	627 [20]	6.5	7.8 [17]	4.6 [17]
Lu	623 [20]			

Fig. 4. Ferrimagnetic structure of a rare-earth iron garnet. The *A*-, *C*- and *D*-positions build up separate magnetic sub-lattices of, whereby the spins are coupled through negative super exchange via the O^{2-} ions. The *A*-lattice ($2Fe^{3+}$-ions) and the *D*-lattice (3 Fe^{3+}-ions) are coupled very strongly, so that at $T = 0$ K the moment of an Fe^{3+} ion results as a ferromagnetic moment. The *C*–*D* coupling is very weak compared to the *A*–*D* coupling.

The cations present in $R_3Fe_5O_{12}$ are thus distributed as

$3R^{3+}$—dodecahedral (*c*) sites,
$3Fe^{3+}$—tetrahedral (*a*) sites,
$2Fe^{3+}$—octahedral (*b*) sites.

All cations are thus in fixed positions with no degrees of freedom, while oxygen anions are in general position, with three degrees of positional freedom. Not all the sites of a given type are crystallographically equivalent. For instance there are six different *c* sites. The ions La^{3+}, Ce^{3+}, Pr^{3+} and Nd^{3+} are too large to form simple garnets but may form solid solutions with other rare-earth garnets.

An adequate picture of the magnetic interactions in RIG could be obtained by the magnetic measurements by Pauthenet [25–27] and Aleonard [28]. The Fe^{3+} ions on the *a* sites are strongly coupled antiferrimagentically to those of the *d* sites. The resultant magnetization of these two sublattices is in turn antiferromagnetically coupled to the spins of the R^{3+} ions on the *c* sites. The magnitude of the Fe–Fe interaction is stronger than the *R*–Fe interactions. The coupling between the *a* and *d* sites is responsible for the Curie temperature at about 550 K, which is approximately same for all the RIG. The coupling of magnetic moments is shown in Fig. 4. The net magnetic moment per formula unit could be given by

$$\mu_{net} = 3\mu(R^{3+})^{dod} - 3\mu(Fe^{3+})^{tet} + 2\mu(Fe^{3+})^{oct}$$
$$= 3\mu(R^{3+})^{dod} - \mu(Fe^{3+})^{tet}. \qquad (1)$$

Below 70 K, the Fe^{3+} ions on the *a* and *d* sites are nearly aligned and the effective molecular field (MF) acting on the Fe^{3+} ion is of the order of 5×10^6 G. In contrast, the MF acting on the R^{3+} ions on the *c* sites is of the order of 2×10^5 G, which produces energy level splitting of the order of 20–50 cm^{-1}.

The magnetic ions are also subjected to a crystalline electric field. For *S*-state R^{3+} ions, the effect of the crystalline field is negligible in comparison to that of the exchange field. When the R^{3+} is not in an *S*-state, the
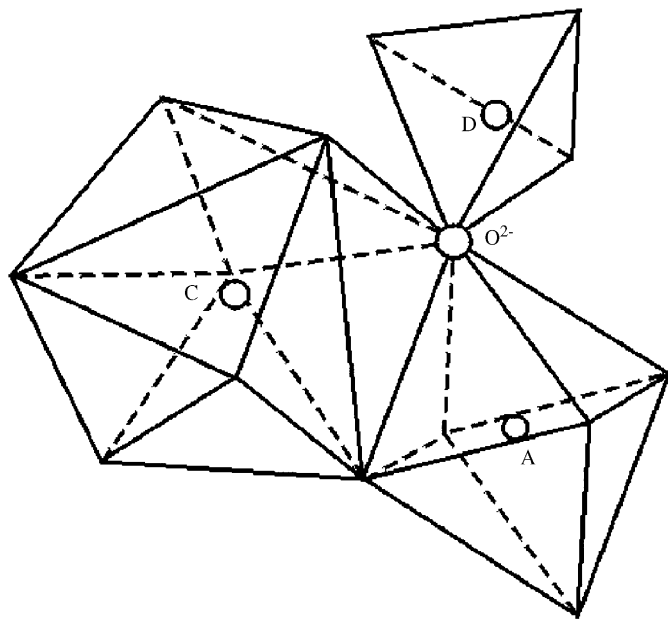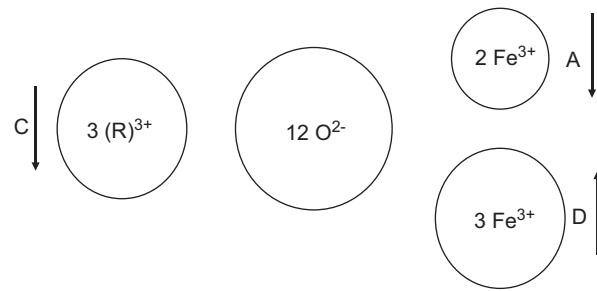

Fig. 3. Crystal structure of garnets: The corners of the polyhedron are occupied with O^{2-}. The cations in the *D*-positions have tetrahedral, in the *A*-positions octahedral and in the *C*-positions pseudo-dodecahedral environment.

The structure of rare-earth iron garnets is described by a body centered unit cell with space group $Ia3d(230)$, containing eight formula units (160 atoms). In the Wyckoff notation, R^{3+} cations occupy special position *c* (24 dodecahedrally co-ordinated sites), whereas Fe^{3+} cations share special positions *a* (sixteen tetrahedrally co-ordinated sites) and *d* (24 octahedrally co-ordinated sites).

crystalline field splitting is of the same order as the exchange splitting. Therefore the magnetic moment of each level will be different from that of the free ion, and in general anisotropic. Under these conditions the number of effectively inequivalent c sites is reduced from six to two at sufficiently low temperatures, and hence one expects different splitting for each level. The levels of R^{3+} split by the exchange field will be appreciably populated above 4 K and will give a large contribution to the heat capacity.

2. Experimental

2.1. Preparation of $RFeO_3(s)$, $R_3Fe_5O_{12}(s)$

The citrate–nitrate gel combustion method was followed for the preparation of $RFeO_3(s)$ and $R_3Fe_5O_{12}(s)$. Preheated $R_2O_3(s)$ (LEICO Industries Inc., USA, 0.999 mass fraction), ferrous ammonium sulfate (Mohr's salt; Qualigens Fine Chemicals, Mumbai, 0.99 mass fraction) were used as the starting materials. The Mohr's salt was dissolved in conc. HNO_3 in order to completely oxidize Fe^{2+} ions to Fe^{3+} ions and then diluted to ~6 M. Stoichiometric amount of preheated $R_2O_3(s)$ was dissolved in dilute HNO_3. Both the solutions were mixed and excess amount of citric acid (E. Merck, India, 0.995 mass fraction) was added to the solution to assist complete dissolution. The solution was heated on a hot plate at around $T = 375$ K to remove water and oxides of nitrogen. A gel was formed which was heated at $T = 450$ K to dryness. The residue was ground in an agate mortar, made into pellets at a pressure of 100 MPa using a steel die and heated at $T = 1473$ K in air in a platinum crucible for 72 h with two intermediate grindings. The products obtained were identified by X-ray diffraction analysis using a DIANO X-ray diffractometer with $CuK\alpha$ radiation ($\lambda = 1.54178$ Å) using a graphite monochromator and found to be single phases.

2.2. Measurement of heat capacity by differential scanning calorimetry (DSC)

The heat flux DSC (Model: DSC 131) supplied by M/s. SETARAM Instrumentations, France, was used to measure the heat capacities of all the samples. The transducer of DSC 131 has been designed using the technology of the plate-shaped DSC rods made of chromel-constantan. It is arranged in a small furnace with a metal resistor of low-thermal inertia so as to produce high heating and cooling rates, thereby providing for high-speed experiments. The transducer also possesses very good sensitivity over the whole temperature range (100–950 K). The temperature calibration of the calorimeter was carried out in the present study by the phase transition temperatures of National Institute of Standards and Technology (NIST) reference materials (mercury: $T_{fus} = 234.316$ K; gallium: $T_{fus} = 302.914$ K; indium: $T_{fus} = 429.748$ K; tin:

$T_{fus} = 505.078$ K; lead: $T_{fus} = 600.600$ K) and AR grade samples (n-pentane: $T_{fus} = 140.490$ K; cyclohexane: $T_{trs} = 190.0$ K; $T_{fus} = 280.1$ K; deionised water: $T_{fus} = 273.160$ K, potassium nitrate: $T_{trs} = 400.850$ K; silver sulfate: $T_{trs} = 703.150$ K; potassium sulfate: $T_{trs.} = 856.150$ K). Heat calibration of the calorimeter was carried out by using the enthalpies of transition of the above mentioned materials. For the determination of heat capacity, NIST synthetic sapphire (SRM 720) in the powder form was used as the reference material. Heat capacity of all the oxides were determined by the Classical three-step method in the continuous heating mode in two different temperature ranges: (i) $130 \leqslant T/K \leqslant 320$ and (ii) $300 \leqslant T/K \leqslant 860$. Heat flow as a function of temperature was measured in the first temperature range at a heating rate of 5 K min^{-1} with high-purity helium as a carrier gas with a flow rate of 2 dm^3 h^{-1}. For the second temperature range, high-purity argon was used as a carrier gas with the same flow rate as that of helium and same heating rate. Two flat bottom aluminum crucibles of identical masses of capacity 10^{-4} dm^3 with covering lids were used as containers for sample and reference materials. About 300–350 mg of the sample was used for the heat capacity measurements. The accuracy and reproducibility of measurements were checked by measuring the heat capacities of Fe_2O_3 (mass fraction 0.998) and NiO (mass fraction 0.999) and found to be within $\pm 2\%$ of the literature values.

3. Results and discussion

3.1. Heat capacity measurements on $RFeO_3(s)$

Heat capacities of $RFeO_3(s)$ (R = La, Nd, Sm, Eu, Gd, Tb, Dy, Ho, Er, Tm, Yb and Lu) have been measured in two different temperature ranges: (i) 130–320 K and (ii) 300–860 K. The experimental heat capacities of these compounds are shown in Fig. 5 in the entire temperature range of 130–860 K.

Heat capacity anomalies have been observed for all the compounds in the temperature range 600–750 K, resembling the λ-type transition. From the earlier studies on the orthoferrites, it has been observed that the phase transition is second order in nature and involves magnetic order-disorder transition from AF to paramagnetic state characterized by the Néel temperature (T_N). The values of T_N for $RFeO_3(s)$ observed from the heat capacity plot shown in Fig. 5 are found to be 724, 697, 675, 664, 663, 652, 647, 644, 642, 634, 629 and 627 K against the literature [20] values of 740, 687, 674, 662, 657, 647, 645, 639, 636, 632, 627 and 623 K for R = La, Nd, Sm, Eu, Gd, Tb, Dy, Ho, Er, Tm, Yb and Lu, respectively, which show good agreement except for $LaFeO_3(s)$. The values are compared in Fig. 6. It can be seen from Fig. 6 that the values of T_N show a systematic decreasing trend with decreasing the ionic radii of R^{3+} ions as one goes from $LaFeO_3$ to $LuFeO_3$. This trend is expected on the basis of increasing structural distortion as discussed in Section 2.
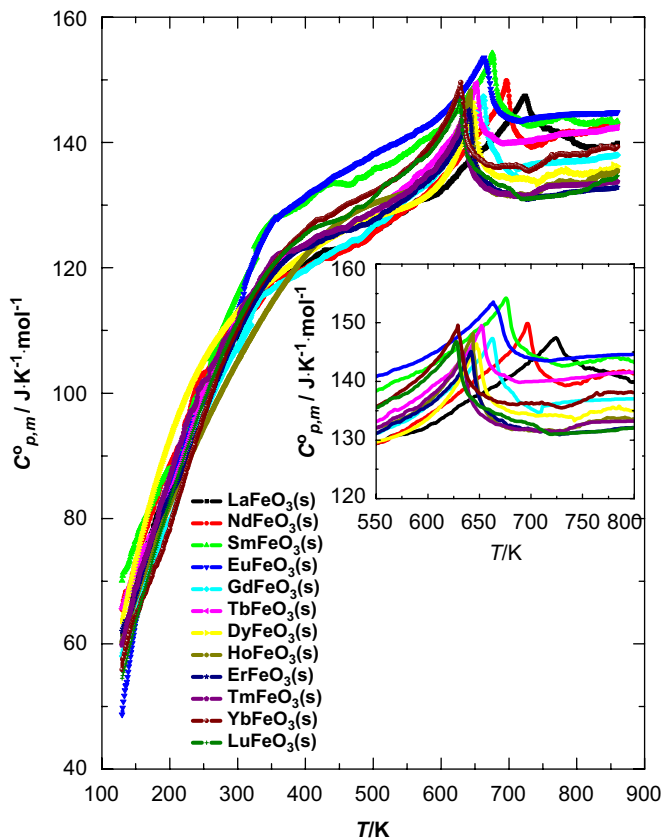
Fig. 5. Plot of molar heat ($C_{p,m}^o$) of RFeO$_3$(s) (R = La, Nd, Sm, Eu, Gd, Tb, Dy, Ho, Er, Tm, Yb and Lu) against temperature (T). The inset shows the magnified portion of the heat capacity plot near the transition region indicating distinct values of Néel temperatures for different RFeO$_3$(s).
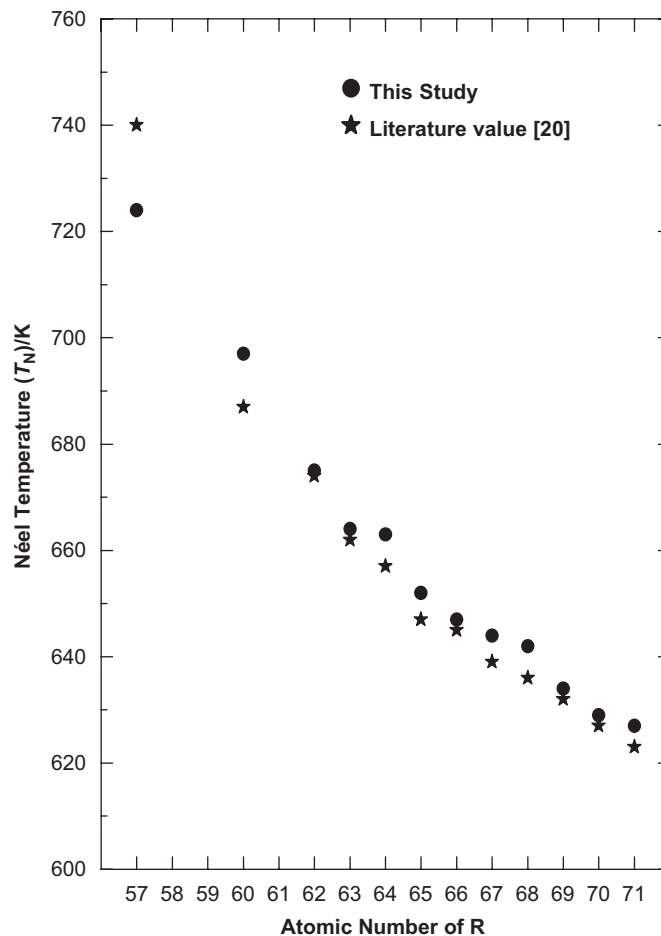

Fig. 6. Comparison of Néel temperatures of RFeO$_3$(s).

The heat capacity data obtained in the present study in the temperature range 130–860 K are combined with the very low-temperature heat capacity data using spline fitting procedure in order to get smooth values of $C_{p,m}^o$ for RFeO$_3$(s) in the entire temperature range from 0 to 860 K (see Supplementary information for tabulated values and figures). These smoothed values are used for further calculations of thermodynamic properties of individual orthoferrites. A detailed discussion of heat capacity, magnetic ordering, calculation of Debye temperature and magnetic entropy associated with order–disorder transitions for each compound is provided below.

3.1.1. LaFeO$_3$(s)

Stølen et al. [21] have measured the heat capacity of LaFeO$_3$(s) in the temperature range from 13 to 900 K using adiabatic calorimetry. They [21] have observed order–disorder transition with T_N = 735 K and derived the thermodynamic functions for LaFeO$_3$(s) from 0 to 900 K using the heat capacity data. The heat capacity data obtained in the present study are in good agreement with those of Stølen et al. [21]. The smoothed values of of $C_{p,m}^o$ for LaFeO$_3$(s) calculated in the present study are shown in Fig. 7(a) as a function of temperature. The lattice heat

capacity of LaFeO$_3$(s) have been calculated by the approximation of Stølen et al. [21] according to which the lattice contribution can be obtained by adding the lattice contributions of the component oxides. The lattice contributions to the heat capacity of the component oxides La$_2$O$_3$(s) and Fe$_2$O$_3$(s) have been taken from the literature [29–32]. This approximation has been tested in the present study for the estimation of lattice heat capacities of NdGaO$_3$(s) and LaAlO$_3$(s) and it was found to be in good agreement with the experimental values [33]. The lattice heat capacity of LaFeO$_3$(s) calculated in this way is shown in Fig. 7(a). The magnetic contribution to the heat capacity of LaFeO$_3$(s) is calculated by using the relation:

$$C_{\text{magnetic}}(\text{LaFeO}_3) = C_{p,m}^o(\text{LaFeO}_3) - \tfrac{1}{2}[C_{\text{lattice}}(\text{Fe}_2\text{O}_3) + C_{\text{lattice}}(\text{La}_2\text{O}_3) + C_{\text{dilational}}(\text{Fe}_2\text{O}_3) + C_{\text{dilational}}(\text{La}_2\text{O}_3)]. \quad (2)$$

The dilational heat capacity of Fe$_2$O$_3$(s) has been taken from Ref. [32] whereas that for La$_2$O$_3$(s) is neglected because of the unavailability of experimental data. However, this will cause a maximum error of $\pm 1\%$, which is

a

b

c
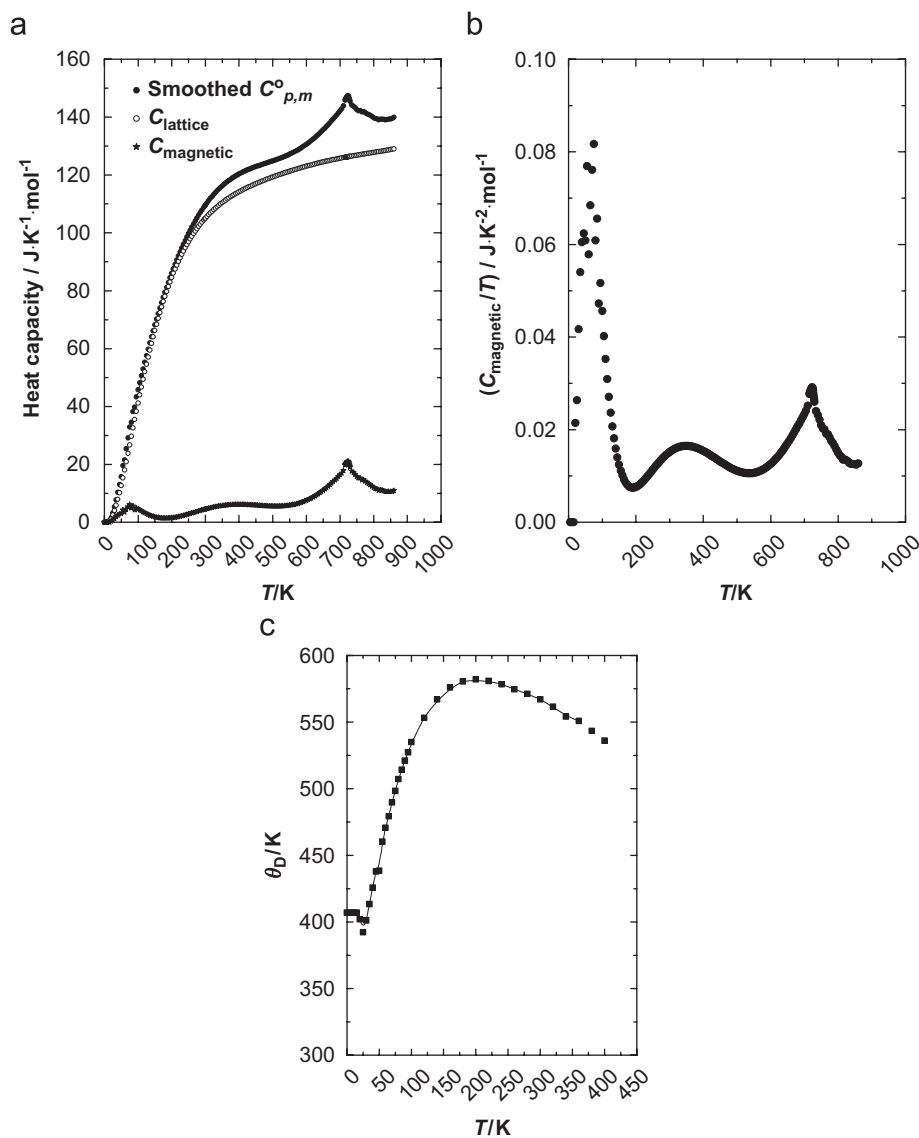
Fig. 7. (a) Plot of $C_{p,m}^o$ against T for LaFeO₃(s); (b) plot of ($C_{magnetic}/T$) against T for LaFeO₃(s); and (c) plot of Debye temperature (θ_D) against temperature (T) for LaFeO₃(s).

well within the uncertainty limit of our estimation method. The magnetic heat capacity for LaFeO₃(s) calculated in this way is shown in Fig. 7(a).

The entropy of transition due to magnetic order–disorder transition can be calculated by integrating the plot of ($C_{magetic}/T$) against T in the temperature range from 0 K to the high temperature tail of the λ-peak. Such a plot for LaFeO₃(s) is shown in Fig. 7(b) and the value of magnetic entropy ($S_{magnetic}$) obtained by integrating the area of the plot is $17.5\,\mathrm{J\,K^{-1}\,mol^{-1}}$. This value is in good agreement with the value obtained form the formula $S_{magnetic} = R\ln(2S+1)$. For LaFeO₃(s) this value becomes $14.897\,\mathrm{J\,K^{-1}\,mol^{-1}}$ because for Fe^{3+} (d^5 electronic configuration) in high spin state, $S = \frac{5}{2}$.

The Debye temperatures (θ_D) as a function of absolute temperature (T) for LaFeO₃(s) are calculated using the tabulated values of Debye function. The plot of the Debye

temperatures (θ_D) against the absolute temperature (T) is shown in Fig. 7(c). The value of θ_D at 0 K is found to be 407 K whereas the effective Debye temperature is found to be 582 K.

3.1.2. NdFeO₃(s)

Bartolome et al. [11] have measured the heat capacity of NdFeO₃(s) in the temperature range 200 mK to 6 K. They have observed a peak at 1.05 K due to cooperative ordering of Nd^{3+} ion. Parida et al. [34] have derived the heat capacity of NdFeO₃(s) from their enthalpy increment measurements in the temperature range from 300 to 1000 K. It is imperative to mention here that the plot of enthalpy increment against temperature reported by them [34] does not show any discontinuity whereas that of heat capacity against temperature shows the discontinuity suggesting that the transition is second order in nature.

Values of θ_D for $NdFeO_3(s)$ are calculated from those of $LaFeO_3(s)$ using the scaling factor given by the formula:

$$\frac{\theta_D(NdFeO_3)}{\theta_D(LaFeO_3)} = \left(\frac{M_{LaFeO_3}}{M_{NdFeO_3}}\right)^{1/2} \left(\frac{V_{LaFeO_3}}{V_{NdFeO_3}}\right)^{1/3}, \qquad (3)$$

where M and V represent molar mass and molar volume of $RFeO_3(s)$. The values of $\theta_D(T)$ calculated in this way for $NdFeO_3(s)$ are finally de-convoluted to $C_{lattice}(T)$ values again using the Debye function. The magnetic contribution to heat capacity is calculated by the procedure similar to $LaFeO_3(s)$. The magnetic entropy calculated for $NdFeO_3(s)$ is equal to $29.9\,J\,K^{-1}\,mol^{-1}$. The higher value obtained for $NdFeO_3(s)$ compared to $LaFeO_3(s)$ is due to the Schottky contribution arising due to magnetic ordering of Nd^{3+} ion at low temperature as pointed out by Bartolome et al. [11]. The value of θ_D at 0 K is found to be 402 K whereas the effective Debye temperature is found to be 574 K.

3.1.3. $SmFeO_3(s)$ and $EuFeO_3(s)$

Parida et al. [35] have derived the heat capacity of $SmFeO_3(s)$ from their enthalpy increment measurements in the temperature range from 300 to 1000 K and concluded that the transition in $SmFeO_3(s)$ is second order in nature. Heat capacity data for $EuFeO_3(s)$ is not available in the literature. The heat capacity values of $SmFeO_3(s)$ and $EuFeO_3(s)$ measured in this study using DSC in the temperature range from 130 to 860 K are smoothened (see Supplementary information). The lattice and magnetic heat contribution to heat capacity for these compounds could not be calculated because of the unavailability of low temperature heat capacity data.

3.1.4. $GdFeO_3(s)$, $TbFeO_3(s)$, $DyFeO_3(s)$, $HoFeO_3(s)$, $ErFeO_3(s)$, $TmFeO_3(s)$, $YbFeO_3(s)$ and $LuFeO_3(s)$

For all these orthoferrites, procedures for the calculation of lattice and magnetic heat capacities, Debye temperatures and magnetic entropies are same as those used for $LaFeO_3(s)$ and $NdFeO_3(s)$.

Cashion et al. [36] have measured the heat capacity of $GdFeO_3(s)$ in the temperature range from 0.5 to 12 K and observed a peak at 1.47 K due to ordering of Gd^{3+} ions. The entropy associated with this transition is $16.04\,J\,K^{-1}\,mol^{-1}$ which is in accordance with a spin of $S = \frac{7}{2}$ of Gd^{3+}. No other experimental heat capacity data is available in the literature. The total magnetic entropy calculated by integrating the plot of $(C_{magetic}/T)$ against T is equal to $22.8\,J\,K^{-1}\,mol^{-1}$. The higher value obtained for $GdFeO_3(s)$ compared to $LaFeO_3(s)$ is due to the Schottky contribution arising due to magnetic ordering of Gd^{3+} ion at low temperature. The value of θ_D at 0 K is found to be 358 K where as the effective Debye temperature is found to be 555 K.

de Combarieu et al. [12] have determined the heat capacity of $TbFeO_3(s)$ in the temperature range 1.2 to 5 K and observed Tb^{3+} ordering at 3.2 K with an effective spin

of $S = \frac{1}{2}$. The magnetic entropy for such ordering is expected to be $5.8\,J\,K^{-1}\,mol^{-1}$ against the observed value of $4.2\,J\,K^{-1}\,mol^{-1}$. The total magnetic entropy calculated for $TbFeO_3(s)$ in this study is equal to $18.3\,J\,K^{-1}\,mol^{-1}$ which is higher than that for $LaFeO_3(s)$ due to magnetic ordering of Tb^{3+} ions at low temperature. The value of θ_D at 0 K is found to be 356 K whereas the effective Debye temperature is found to be 552 K.

Betron and Sharon [16] have determined the heat capacity of $DyFeO_3(s)$ in the temperature range from 1.2 to 80 K and observed Dy^{3+} ordering at 3.7 K. Parida et al. [37] have derived the heat capacity of $DyFeO_3(s)$ from their experimental enthalpy increment values in the temperature range 300–1000 K. The total magnetic entropy calculated for $DyFeO_3(s)$ in this study is equal to $21.1\,J\,K^{-1}\,mol^{-1}$ which is higher than that for $LaFeO_3(s)$ due to magnetic ordering of Dy^{3+} ions at low temperature. The value of θ_D at 0 K is found to be 352 K whereas the effective Debye temperature is found to be 551 K.

Saito et al. [19] have measured the heat capacity of $HoFeO_3(s)$ in the temperature range from 50 to 70 K. Bhattacharjee et al. [18] have measured the heat capacity of $HoFeO_3(s)$ from 2.8 to 200 K. The total magnetic entropy calculated for $HoFeO_3(s)$ in this study is equal to $25.9\,J\,K^{-1}\,mol^{-1}$ which is higher than that for $LaFeO_3(s)$ due to magnetic ordering of Ho^{3+} ions at low temperature. The value of θ_D at 0 K is found to be 342 K where as the effective Debye temperature is found to be 550 K.

Saito et al. [38] have determined the heat capacity of $ErFeO_3(s)$ in the temperature range from 6 to 300 K. The total magnetic entropy calculated for $ErFeO_3(s)$ in this study is equal to $23.8\,J\,K^{-1}\,mol^{-1}$ which is higher than that for $LaFeO_3(s)$ due to magnetic ordering of Er^{3+} ions at low temperature. The value of θ_D at 0 K is found to be 339 K whereas the effective Debye temperature is found to be 548 K.

Saito et al. [38] have determined the heat capacity of $TmFeO_3(s)$ in the temperature range from 6 to 300 K. In another study Saito et al. [19] have measured the heat capacity in the temperature range from 60 to 110 K. The total magnetic entropy calculated for $TmFeO_3(s)$ in this study is equal to $19.2\,J\,K^{-1}\,mol^{-1}$ which is higher than that for $LaFeO_3(s)$ due to magnetic ordering of Tm^{3+} ions at low temperature. The value of θ_D at 0 K is found to be 337 K whereas the effective Debye temperature is found to be 544 K.

Moldover et al. [17] have determined the heat capacity of $YbFeO_3(s)$ from 1.5 to 15 K. No other experimental heat capacity data is available in the literature. The total magnetic entropy calculated for $YbFeO_3(s)$ in this study is equal to $18.7\,J\,K^{-1}\,mol^{-1}$ which is higher than that for $LaFeO_3(s)$ due to magnetic ordering of Yb^{3+} ions at low temperature. The value of θ_D at 0 K is found to be 335 K where as the effective Debye temperature is found to be 542 K.

Bhattacharjee et al. [18] have measured the heat capacity of $LuFeO_3(s)$ from 1.8 to 200 K. No other experimental

heat capacity data are available in the literature. The lattice and magnetic heat capacities of $LuFeO_3(s)$ are calculated by the procedure similar to that for $NdFeO_3(s)$. The total magnetic entropy calculated for $LuFeO_3(s)$ in this study is equal to $15.1\,J\,K^{-1}\,mol^{-1}$, which is in good agreement with the theoretical value of $14.9\,J\,K^{-1}\,mol^{-1}$ on the basis of non-magnetic Lu^{3+} ions. The value of θ_D at 0 K is found to be 333 K whereas the effective Debye temperature is found to be 541 K.

3.2. Heat capacity measurements on $R_3Fe_5O_{12}(s)$

Heat capacities of $R_3Fe_5O_{12}(s)$ (R = Sm, Eu, Gd, Tb, Dy, Ho, Er, Tm, Yb and Lu) have been measured in two different temperature ranges: (i) 130–320 K and (ii) 300–860 K. The experimental heat capacities of these compounds are shown in Fig. 8 in the entire temperature range 130–860 K.

Heat capacity anomalies have been observed for all the compounds in the temperature range 530–560 K, resembling the λ-type transition. From the earlier studies on the rare-earth iron garnets (RIG), it has been observed that the phase transition is second order in nature and involves magnetic order–disorder transition from ferrimagnetic to paramagnetic state characterized by the Curie temperature (T_C). The values of T_C for $R_3Fe_5O_{12}(s)$ observed from the heat capacity plot shown in Fig. 8 are found to be 567, 559, 556, 556, 554, 544, 543, 540 and 537 K for R = Sm, Eu, Gd, Tb, Dy, Ho, Er, Tm, Yb and Lu, respectively. The reported literature values [26] of T_C are 565, 563, 560, 556, 551, 549 and 531.5 K for R = Sm, Eu, Gd, Tb, Dy, Er and Lu, respectively. The values are compared in Fig. 9. It can be seen from Fig. 9 that the values of T_C for $R_3Fe_5O_{12}$ show a systematically decreasing trend with decrease in ionic radii of R^{3+} ions as one goes from $Sm_3Fe_5O_{12}$ to $Lu_3Fe_5O_{12}$. However, this decrease is not significant compared to that observed for $RFeO_3$. This can be explained on the basis of structural differences between these two classes of compound.

Harris and Meyer [39] have measured the low temperature heat capacities of $R_3Fe_5O_{12}(s)$ (R = Sm, Gd, Tb, Dy, Ho, Er, Yb and Lu) from 1.3 to 20.6 K and calculated the Schottky levels of these compounds from the heat capacity data. Henderson et al. [40] have measured the heat capacities of RIGs for R = Eu, Tm, Sm and Yb from 0.4 to 4.2 K and deduced the Debye temperatures of these compounds at 0 K. Varazashvili et al. [41] have measured the heat capacities of RIGs for R = Sm, Eu, Gd, Tb, Dy
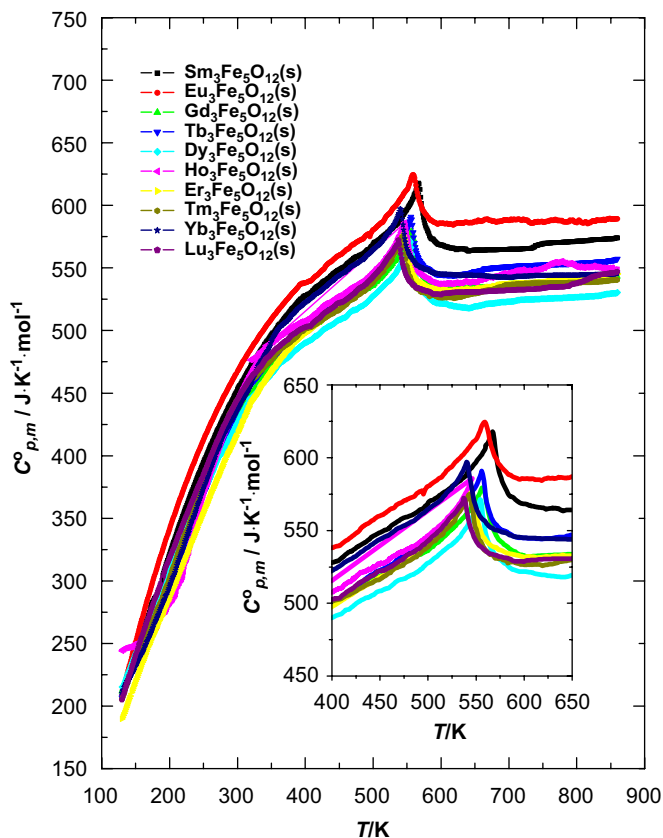
Fig. 8. Plot of molar heat capacities ($C^o_{p,m}$) of $R_3Fe_5O_{12}(s)$ (R = Sm, Eu, Gd, Tb, Dy, Ho, Er, Tm, Yb and Lu) against temperature (T). The inset shows the magnified portion of the heat capacity plot near the transition region indicating nearly same values of Curie temperatures for different $R_3Fe_5O_{12}(s)$.
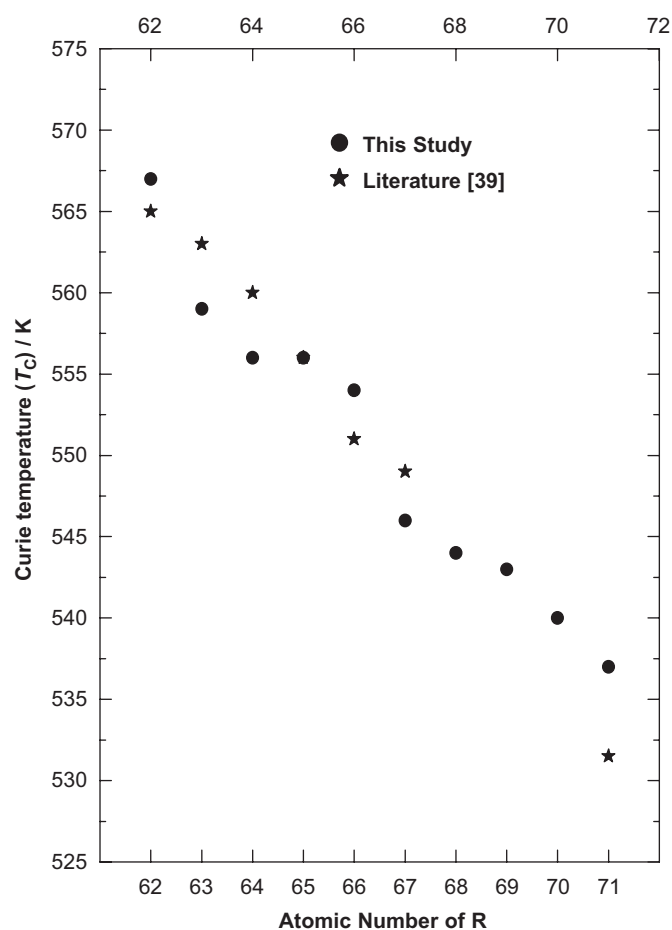

Fig. 9. Comparison of Curie temperatures (T_C) for $R_3Fe_5O_{12}(s)$.

Table 3
Magnetic splitting energies of RIGs

$R_3Fe_5O_{12}$	$\overline{E1}/cm^{-1}$	$\overline{E2}/cm^{-1}$
$Sm_3Fe_5O_{12}$	38.873	–
$Eu_3Fe_5O_{12}$	99.022	–
$Gd_3Fe_5O_{12}$	26.826	–
$Tb_3Fe_5O_{12}$	37.000	109.340
$Dy_3Fe_5O_{12}$	28.764	72.396
$Ho_3Fe_5O_{12}$	30.312	53.999
$Er_3Fe_5O_{12}$	20.011	37.576
$Tm_3Fe_5O_{12}$	37.040	109.340
$Yb_3Fe_5O_{12}$	25.000	–
$Lu_3Fe_5O_{12}$	67.753	–

and Er from 300 to 850 K. Mirianashvilli et al. [42] have measured the heat capacity of $Lu_3Fe_5O_{12}$(s) from 300 to 900 K. Varazashvilli et al. [43] have measured the low temperature heat capacities of $Gd_3Fe_5O_{12}$(s) and $Lu_3Fe_5O_{12}$(s) from 20 to 300 K. Moretti and Ottonello [44] have calculated the Schottky levels and tabulated the thermodynamic functions of all the RIGs based on the available literature data. Parida et al. [35,37] have measured the enthalpy increments of $Sm_3Fe_5O_{12}$(s) and $Dy_3Fe_5O_{12}$(s) from 300 to 1000 K and derived the heat capacities. They have concluded that the magnetic order–disorder transitions in these compounds are second order in nature. The heat capacity data obtained in the present study are combined with the literature data and smoothened using the spline fitting procedure in order to get $C_{p,m}^o$ values from 0 to 850 K. The smoothed values are given in the Supplementary information.

The lattice contribution to heat capacities for all these compounds is calculated by the procedure similar to that for $RFeO_3$(s). The Schottky contribution to heat capacities is calculated by using the equation given by Moretti and Ottonello [44] as shown below:

$$\Delta C_{Schottky} = 3R\left\{\left(\frac{\overline{E1}}{k_BT}\right)^2\left[\frac{\exp(-\overline{E1}/k_BT)}{[1+\exp(-\overline{E1}/k_BT)]^2}\right] \right.$$
$$\left. +\left(\frac{\overline{E2}}{k_BT}\right)^2\left[\frac{\exp(-\overline{E2}/k_BT)}{[1+\exp(-\overline{E2}/k_BT)]^2}\right]\right\}. \quad (4)$$

The values of $\overline{E1}$ and $\overline{E2}$ are taken from Moretti and Ottonello [44] and listed in Table 3.

The dilational contribution is found to be negligible and hence not included in the calculation. The magnetic contribution to heat capacity is found out by subtracting all other contribution from the measured $C_{p,m}^o$. The magnetic entropy is derived by integrating the plot of $(C_{magnetic}/T)$ against T. The values of magnetic entropies ($S_{magnetic}$) obtained in the present study are: 107.6, 113.0, 81.8, 62.6, 107.8, 82.7, 108.0, 96.2 and 78.3 J K^{-1} mol^{-1} for $R =$ Sm, Gd, Tb, Dy, Ho, Er, Tm, Yb and Lu, respectively.

The Debye temperatures are derived by the procedure similar to $RFeO_3$(s). The values of $C_{p,m}^o$, $C_{lattice}$, $C_{Schottky}$, $C_{magnetic}$, $(C_{magnetic}/T)$ and θ_D as a function of absolute temperature T are shown in Figs. 10(a)–(d) for the compound $Sm_3Fe_5O_{12}$(s) (See Supplementary information for other RIGs). Such type of calculations could not be performed for $Eu_3Fe_5O_{12}$(s) because of the unavailability of low temperature heat capacity data with sufficient accuracy.

3.3. Construction of thermodynamic tables for $RFeO_3$(s) and $R_3Fe_5O_{12}$(s)

The values of $S_m^o(298.15\,K)$ and $\Delta_f H_m^o(298.15\,K)$ are generally calculated by two different methods; the second-law method and the third-law method. For the calculation of $S_m^o(298.15\,K)$ by the third-law method, the heat capacity data for the compounds from 0 K to temperatures above 298.15 K are required. The low-temperature heat capacity data for $SmFeO_3$(s), $EuFeO_3$(s) and $Eu_3Fe_5O_{12}$(s) are not available. Hence for all the $RFeO_3$(s) and $R_3Fe_5O_{12}$(s) compounds except these three oxides, the $S_m^o(298.15\,K)$ values have been calculated by the third-law method.

Similarly, for the calculation of $\Delta_f H_m^o(298.15\,K)$ by third law method, the absolute values of $S_m^o(298.15\,K)$, the values of $\{H_m^o(T)-H_m^o(298.15\,K)\}$ or $C_{p,m}^o(T)$ and $\Delta_f G_m^o(T)$ are required. For accurate values of $\Delta_f H_m^o(298.15\,K)$, the heat capacity values should be measured up to the temperature where experimental values of $\Delta_f G_m^o(T)$ are available. However, in the present study the heat capacity values are measured up to 860 K whereas the experimental values of $\Delta_f G_m^o(T)$ are available above 1000 K. Hence, the heat capacity of $RFeO_3$(s) and $R_3Fe_5O_{12}$(s) have been extrapolated above 860 K up to 1300 K, in order to calculate $\Delta_f H_m^o(298.15\,K)$ by the third law method. However, for $SmFeO_3$(s), $EuFeO_3$(s) and $Eu_3Fe_5O_{12}$(s), third law calculations could not be performed because the absolute values of $S_m^o(298.15\,K)$ are not known.

The entropy increment $\{S_m^o(T)-S_m^o(0)\}$ and the enthalpy increment $\{H_m^o(T)-H_m^o(0)\}$ functions have been calculated by numerical integration of the $C_p^o(T)/T$ and $C_p^o(T)$ functions, respectively. These functions have been constructed using polynomial fit of the $C_p^o(T)$ curve in small temperature ranges. The Gibbs energy, $\{G_m^o(T)-H_m^o(0)\}$ has been calculated by using the relation:

$$\{G_m^o(T)-H_m^o(0)\} = \{H_m^o(T)-H_m^o(0)\} - TS_m^o(T). \quad (5)$$

The values of $\{H_m^o(T)-H_m^o(298.15\,K)\}$ have been calculated by using the relation

$$\{H_m^o(T)-H_m^o(298.15\,K)\} = \{H_m^o(T)-H_m^o(0)\}$$
$$- \{H_m^o(298.15\,K)-H_m^o(0)\}. \quad (6)$$

In order to make full use of the thermodynamic data, $G_m^o(T)$ should be evaluated which requires a known value of $H_m^o(0)$. However, absolute value of $H_m^o(0)$ is difficult to
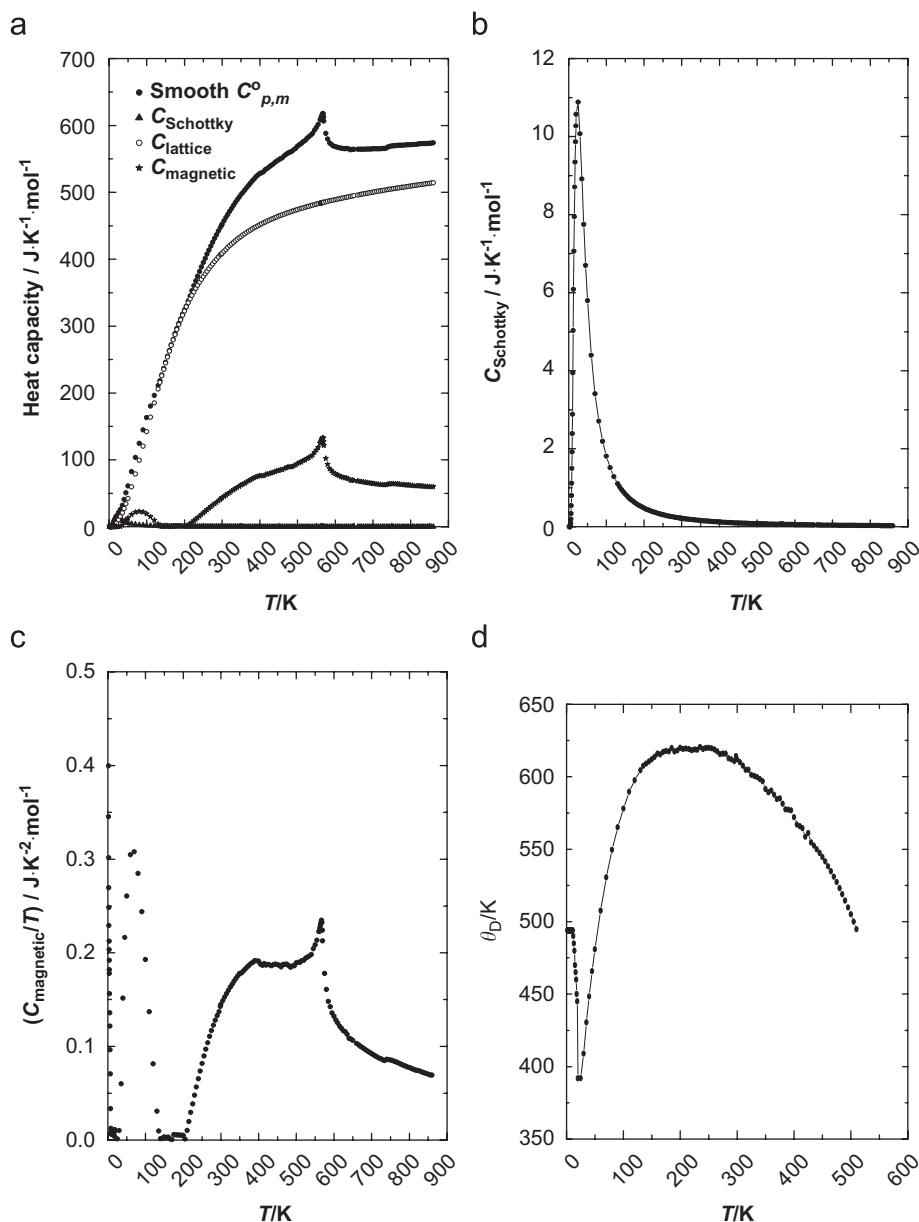
Fig. 10. (a) Plot of heat capacity against T for $Sm_3Fe_5O_{12}(s)$; (b) plot of $C_{electronic}$ against T for $Sm_3Fe_5O_{12}(s)$; (c) plot of $(C_{magnetic}/T)$ against T for $Sm_3Fe_5O_{12}(s)$; and (d) plot of (θ_D) against the absolute temperature (T) for $Sm_3Fe_5O_{12}(s)$.

determine or calculate. Therefore, first $H_m^o(T)$ has been calculated using the relation:

$$H_m^o(T) = \Delta_f H_{298.15\,K}^o + \int_{298.15}^{T} C_{p,m}^o(T)\,dT. \qquad (7)$$

The absolute value of $S_m^o(T)$ has been calculated using $S_m^o(0) = 0$ and the relation:

$$S_m^o(T) = \int_0^T \frac{C_{p,m}^o(T)}{T}\,dT. \qquad (8)$$

Now $G_m^o(T)$ can be calculated using the relation

$$G_m^o(T) = H_m^o(T) - TS_m^o(T). \qquad (9)$$

The free energy function (or the Plank's function) $\Phi_m^o(T)$ has been calculated using the relation

$$\Phi_m^o(T) = -\left\{ \frac{G_m^o(T) - H_m^o(298.15\,K)}{T} \right\}. \qquad (10)$$

After calculation of all the thermodynamic functions, the values have been tabulated at selected temperatures. The thermodynamic functions which are usually tabulated in tables are: $C_{p,m}^o$, S_m^o, $\{H_m^o(T) - H_m^o(298.15\,K)\}$, H_m^o, $\Phi_m^o(T)$, $\Delta_f H_m^o(T)$ and $\Delta_f G_m^o(T)$. The values generated in this study for $RFeO_3(s)$ (R = La, Nd, Sm, Eu, Gd, Tb, Dy, Ho and Eu) and $R_3Fe_5O_{12}(s)$ (R = Sm, Eu, Gd, Tb, Dy, Ho and Eu) are listed in Tables 4–20. Tables for other $RFeO_3(s)$ and $R_3Fe_5O_{12}(s)$ compounds has not been

Table 4
Values of $\theta_{D(0\,K)}$, $\theta_{D(effective)}$ and $S_{(magnetic)}$ for $RFeO_3(s)$ and $R_3Fe_5O_{12}(s)$

Perovskite	$\theta_{D(0\,K)}$/K	$\theta_{D(effective)}$/K	$S_{(magnetic)}$/J K^{-1} mol^{-1}	Garnet	$\theta_{D(0\,K)}$/K	$\theta_{D(effective)}$/K	$S_{(magnetic)}$/J K^{-1} mol^{-1}
LaFeO$_3$	407	582	17.5	–			
NdFeO$_3$	402	574	29.9	–			
SmFeO$_3$	–	–	–	Sm$_3$Fe$_5$O$_{12}$	494	662	107.6
EuFeO$_3$	–	–	–	Eu$_3$Fe$_5$O$_{12}$	–	–	–
GdFeO$_3$	358	555	22.8	Gd$_3$Fe$_5$O$_{12}$	490	655	113.0
TbFeO$_3$	356	552	18.3	Tb$_3$Fe$_5$O$_{12}$	455	656	81.8
DyFeO$_3$	352	551	21.1	Dy$_3$Fe$_5$O$_{12}$	422	657	62.6
HoFeO$_3$	342	550	25.9	Ho$_3$Fe$_5$O$_{12}$	419	646	107.8
ErFeO$_3$	339	548	23.8	Er$_3$Fe$_5$O$_{12}$	418	648	82.7
TmFeO$_3$	337	544	19.2	Tm$_3$Fe$_5$O$_{12}$	414	645	108.0
YbFeO$_3$	335	542	18.7	Yb$_3$Fe$_5$O$_{12}$	414	646	96.2
LuFeO$_3$	333	541	15.1	Lu$_3$Fe$_5$O$_{12}$	392	650	78.3

Table 5
Thermodynamic data for LaFeO$_3$(s)

T/K	S_T°/ J K^{-1} mol^{-1}	$C_{p,m}^\circ$/ J K^{-1} mol^{-1}	$H_T^\circ - H_0^\circ$/ J mol^{-1}	$H_T^\circ - H_{298.15}^\circ$/ J mol^{-1}	$-H_T^\circ$/ J mol^{-1}	$-G_T^\circ$/ J mol^{-1}	$-(G_T^\circ - H_{298.15}^\circ)/T$/ J K^{-1} mol^{-1}	$-\Delta_f H_m^\circ$/ kJ mol^{-1}	$-\Delta_f G_m^\circ$/ kJ mol^{-1}
0	0	0	0						
25	0.920	3.204	17.8940						
50	6.770	15.70	247.059						
75	16.26	31.94	846.401						
100	27.40	45.78	1822.41						
150	50.35	68.16	4690.07						
200	72.52	85.94	8564.44						
250	93.23	99.55	13,219.0						
298.15	111.6	106.4	18,253.3	0	1,377,200	1,410,473	111.6	1372.6	1291.7
300	112.2	106.7	18,448.8	195.4	1,377,002	1,410,681	111.6	1372.6	1291.7
325	120.9	110.2	21,148.1	2894.8	1,374,291	1,413,596	112.0	1372.7	1285.0
350	129.2	113.2	23,927.8	5674.4	1,371,498	1,416,724	113.0	1372.6	1278.3
400	144.7	118.4	29,693.3	11,440.0	1,365,705	1,423,577	116.1	1372.3	1264.8
450	158.9	123.1	35,693.0	17,440.6	1,359,668	1,431,171	120.1	1371.9	1251.4
500	172.1	127.7	41,907.7	23,654.4	1,353,400	1,439,450	124.8	1373.5	1238.0
550	184.5	132.6	48,342.2	30,088.9	1,346,894	1,448,368	129.8	1372.2	1224.5
600	196.3	138.4	55,034.6	36,781.3	1,340,122	1,457,889	134.9	1371.1	1211.1
650	207.6	145.8	62,051.4	43,798.1	1,333,025	1,467,989	140.3	1369.5	1197.8
700	218.8	156.3	69,488.5	51,235.2	1,325,489	1,478,650	145.6	1367.6	1184.7
724	224.2	163.2	73,243.3	54,990.0	1,321,658	1,483,965	148.2	1366.5	1178.5
724	224.2	163.2	73,243.3	54,990.0	1,321,658	1,483,965	148.2	1366.5	1178.5
750	229.1	137.8	76,869.0	58,615.7	1,318,034	1,489,858	150.9	1365.9	1171.7
800	237.9	134.8	83,681.6	65,428.3	1,311,230	1,501,536	156.1	1365.0	1158.8
850	246.0	133.7	90,381.6	72,128.3	1,304,520	1,513,636	161.2	1364.4	1145.9
900	253.7	133.5	97,049.8	78,796.5	1,297,542	1,526,130	166.1	1364.0	1133.1
950	260.9	133.6	103,727	85,473.8	1,291,167	1,538,994	170.9	1363.8	1120.3
1000	267.7	133.9	110,414	92,161.0	1,284,481	1,552,211	175.6	1364.0	1107.5

constructed in this study because of the unavailability of auxiliary thermodynamic data in the literature.

4. Conclusions

Ternary oxides $RFeO_3(s)$ and $R_3Fe_5O_{12}(s)$ having magnetic properties are prepared by citrate-nitrate gel combustion method and characterized by X-ray diffraction method. Heat capacities of these compounds are measured from 130 to 860 K using differential scanning calorimeter. Heat capacity anomalies are observed for all these compounds. The heat capacity anomaly for the rare-earth orthoferrites $RFeO_3(s)$ observed in the temperature range of 600–725 K are assigned due to magnetic order–disorder transformation from antiferromagnetic to paramagnetic state. It has also been observed that the transition temperature (Néel temperature, T_N) for these compounds shows a systematic decreasing trend from La to Lu. The

Table 6
Thermodynamic data for NdFeO$_3$(s)

T/K	S°_T/ J K^{-1} mol^{-1}	$C^\circ_{p,m}$/ J K^{-1} mol^{-1}	$H^\circ_T - H^\circ_0$/ J mol^{-1}	$H^\circ_T - H^\circ_{298.15}$/ J mol^{-1}	$-H^\circ_T$/ J mol^{-1}	$-G^\circ_T$/ J mol^{-1}	$-(G^\circ_T - H^\circ_{298.15})/T$/ J K^{-1} mol^{-1}	$-\Delta_f H^\circ_m$/ kJ mol^{-1}	$-\Delta_f G^\circ_m$/ kJ mol^{-1}
0	0	0							
25	9.327	6.354	74.0060						
50	17.23	17.88	376.482						
75	27.29	32.71	1009.16						
100	38.71	49.03	2010.52						
150	63.65	74.82	5129.55						
200	88.02	90.37	9388.13						
250	109.6	102.9	14,246.3						
298.15	128.5	107.5	19,407.4	0	1,362,200	1,400,512	128.5	1357.4	1278.4
300	129.2	107.7	19,605.9	198.5	1,362,000	1,400,751	128.5	1357.4	1277.9
325	137.9	111.2	22,337.2	2929.7	1,359,263	1,404,090	128.9	1357.5	1271.3
350	146.3	114.3	25,151.6	5744.2	1,356,444	1,407,643	129.9	1357.6	1264.6
400	161.9	119.8	30,996.3	11,588.9	1,350,590	1,415,354	132.9	1357.5	1251.4
450	176.3	124.9	37,095.6	17,688.2	1,344,473	1,423,814	137.0	1359.6	1237.9
500	189.7	130.3	43,441.7	24,034.3	1,338,093	1,432,969	141.7	1358.5	1224.4
550	202.5	136.4	50,063.5	30,656.1	1,331,429	1,442,777	146.7	1357.2	1211.0
600	214.6	143.9	57,026.8	37,619.4	1,324,428	1,453,206	151.9	1355.7	1197.8
650	226.5	154.2	64,434.0	45,026.6	1,316,991	1,464,235	157.3	1354.0	1184.7
697	237.7	168.8	71,925.5	52,518.1	1,309,426	1,475,146	162.4	1351.9	1172.6
697	237.7	168.8	71,925.5	52,518.1	1,309,426	1,475,146	162.4	1351.9	1172.6
700	238.4	142.7	72,358.5	52,951.1	1,308,997	1,475,859	162.7	1351.8	1171.8
750	247.9	136.7	79,431.9	60,024.5	1,302,039	1,488,023	167.9	1350.9	1158.9
800	256.7	134.7	86,329.5	66,922.1	1,295,262	1,500,643	173.1	1350.3	1146.1
850	264.9	133.9	93,161.3	73,753.9	1,288,549	1,513,686	178.1	1350.0	1133.4
900	272.5	133.9	99,998.7	80,591.3	1,281,854	1,527,122	182.9	1350.0	1120.7
950	279.8	134.4	106,874	87,467.0	1,275,153	1,540,931	187.7	1350.2	1107.9
1000	286.7	134.7	113,782	94,375.4	1,268,432	1,555,093	192.3	1350.7	1095.2

Table 7
Thermodynamic data for SmFeO$_3$(s)

T/K	S°_T/ J K^{-1} mol^{-1}	$C^\circ_{p,m}$/ J K^{-1} mol^{-1}	$H^\circ_T - H^\circ_0$/ J mol^{-1}	$H^\circ_T - H^\circ_{298.15}$/ J mol^{-1}	$-H^\circ_T$/ J mol^{-1}	$-G^\circ_T$/ J mol^{-1}	$-(G^\circ_T - H^\circ_{298.15})/T$/ J K^{-1} mol^{-1}	$-\Delta_f H^\circ_m$/ kJ mol^{-1}	$-\Delta_f G^\circ_m$/ kJ mol^{-1}
0	–	–	–						
25	–	–	–						
50	–	–	–						
75	–	–	–						
100	–	–	–						
150	–	–	–						
200	–	–	–						
250	–	–	–						
298.15	128.2	115.4	–	0	1,355,200	1,393,423	128.2	1355.2	1272.9
300	128.9	115.8	–	214	1,354,986	1,393,661	128.2	1355.2	1272.4
325	138.4	120.6	–	3171	1,352,029	1,397,003	128.6	1354.7	1365.5
350	147.5	124.5	–	6236	1,348,964	1,400,576	129.6	1354.2	1258.6
400	164.5	130.4	–	12,616	1,342,584	1,408,382	132.9	1352.9	1245.1
450	180.1	134.7	–	19,247	1,335,953	1,417,002	137.3	1351.7	1231.6
500	194.5	138.2	–	26,072	1,329,128	1,426,372	142.3	1350.4	1218.4
550	207.8	141.3	–	33,060	1,322,140	1,436,433	147.7	1349.1	1205.2
600	220.2	144.5	–	40,204	1,314,996	1,447,138	153.2	1347.8	1192.2
650	231.9	148.4	–	47,522	1,307,678	1,458,445	158.8	1346.6	1179.3
675	237.6	150.9	–	41,803	1,397,003	1,464,315	161.7	1345.9	1172.9
675	237.6	150.9	–	41,803	1,397,003	1,464,315	161.7	1345.9	1172.9
700	242.8	143.7	–	54,863	1,300,337	1,470,320	164.5	1345.6	1166.5
750	252.7	143.1	–	62,029	1,293,171	1,482,712	170.0	1344.7	1153.7
800	261.9	143.0	–	69,181	1,286,019	1,495,582	175.5	1344.1	1141.0
850	270.6	143.1	–	76,334	1,278,866	1,508,898	180.8	1343.8	1128.3
900	278.8	143.2	–	83,492	1,271,708	1,522,636	186.0	1343.6	1115.7
950	286.6	143.3	–	90,656	1,264,544	1,536,772	191.1	1343.8	1102.9
1000	293.9	143.5	–	97,827	1,257,373	1,551,285	196.2	1344.2	1090.3

Table 8
Thermodynamic data for EuFeO$_3$(s)

T/K	S^o_T/ J K^{-1} mol^{-1}	$C^o_{p,m}$/ J K^{-1} mol^{-1}	$H^o_T-H^o_0$/ J mol^{-1}	$H^o_T-H^o_{298.15}$/ J mol^{-1}	$-H^o_T$/ J mol^{-1}	$-G^o_T$/ J mol^{-1}	$-(G^o_T-H^o_{298.15})/T$/ J K^{-1} mol^{-1}	$-\Delta_f H^o_m$/ kJ mol^{-1}	$-\Delta_f G^o_m$/ kJ mol^{-1}
0	–	–	–						
25	–	–	–						
50	–	–	–						
75	–	–	–						
100	–	–	–						
150	–	–	–						
200	–	–	–						
250	–	–	–						
298.15	122.4	112.9	–	0	1,285,600	1,322,094	122.4	1285.6	1199.1
300	123.1	113.4	–	209.2	1,285,390	1,322,321	122.4	1285.1	1198.5
325	132.4	119.2	–	3113.4	1,282,479	1,325,515	122.8	1285.1	1191.3
350	141.4	123.9	–	6143.8	1,279,437	1,328,939	123.9	1284.5	1184.1
400	158.5	130.9	–	12,508.8	1,273,053	1,336,442	127.2	1283.0	1169.8
450	174.2	136.0	–	19,180.0	1,266,370	1,344,765	131.6	1281.4	1155.8
500	188.7	140.0	–	26,071.1	1,259,465	1,353,843	136.6	1279.6	1141.9
550	202.3	143.5	–	33,134.1	1,252,376	1,363,623	142.0	1277.8	1128.3
600	214.9	147.0	–	40,358.7	1,245,114	1,374,056	147.6	1275.9	1114.8
650	226.8	151.3	–	47,773.2	1,237,662	1,385,101	153.3	1273.8	1101.4
664	230.1	152.8	–	49,891.3	1,235,533	1,388,299	154.9	1273.3	1097.7
664	230.1	152.8	–	49,891.3	1,235,533	1,388,299	154.9	1273.3	1097.7
700	237.8	145.4	–	55,137.7	1,230,285	1,396,722	158.9	1272.0	1088.2
750	247.8	144.9	–	62,397.1	1,223,029	1,408,864	164.6	1270.4	1075.1
800	257.1	144.8	–	69,640.7	1,215,785	1,421,489	170.1	1269.0	1062.2
850	265.9	144.8	–	76,880.6	1,208,542	1,434,567	175.5	1267.7	1049.3
900	274.2	144.9	–	84,122.9	1,201,298	1,448,072	180.7	1266.6	1036.5
950	282.0	144.9	–	91,368.2	1,194,055	1,461,979	185.8	1265.6	1023.7
1000	289.5	144.8	–	98,610.9	1,186,813	1,476,268	190.8	1264.9	1011.0

Table 9
Thermodynamic data for GdFeO$_3$(s)

T/K	S^o_T/ J K^{-1} mol^{-1}	$C^o_{p,m}$/ J K^{-1} mol^{-1}	$H^o_T-H^o_0$/ J mol^{-1}	$H^o_T-H^o_{298.15}$/ J mol^{-1}	$-H^o_T$/ J mol^{-1}	$-G^o_T$/ J mol^{-1}	$-(G^o_T-H^o_{298.15})/T$/ J K^{-1} mol^{-1}	$-\Delta_f H^o_m$/ kJ mol^{-1}	$-\Delta_f G^o_m$/ kJ mol^{-1}
0	0	0	0						
25	15.40	3.110	54.2200						
50	21.04	15.99	276.167						
75	30.50	31.63	872.630						
100	41.67	46.93	1852.62						
150	65.64	71.68	4849.84						
200	88.80	88.88	8895.59						
250	109.9	100.0	13,639.8						
298.15	128.2	109.8	18,636.1	0	1,360,500	1,398,723	128.2	1360.5	1278.6
300	128.9	110.1	18,838.3	202.2	1,360,296	1,398,961	128.2	1360.4	1278.1
325	137.8	113.4	21,626.1	2990.0	1,357,501	1,402,295	128.6	1360.3	1271.3
350	146.3	116.4	24,494.8	5858.7	1,354,629	1,405,848	129.6	1359.9	1264.4
400	162.2	121.8	30,440.3	11804.2	1,348,673	1,413,569	132.7	1359.0	1250.8
450	176.9	127.1	36,637.6	18001.5	1,342,452	1,422,052	136.9	1357.9	1237.4
500	190.6	132.9	73,092.4	24456.3	1,335,954	1,431,241	141.7	1356.5	1224.1
550	203.6	139.8	49,857.5	31221.4	1,329,142	1,441,097	146.8	1354.9	1210.9
600	216.1	149.1	57,032.3	38396.2	1,321,932	1,451,589	152.1	1353.2	1197.9
650	222.3	162.9	64,761.2	46125.1	1,314,158	1,462,705	157.6	1350.9	1185.0
663	231.8	167.9	66,883.9	48247.8	1,312,009	1,465,697	159.0	1350.2	1181.7
663	231.8	167.9	66,883.9	48247.8	1,312,009	1,465,697	159.0	1350.2	1181.7
700	239.4	136.8	72,046.0	53,409.9	1,306,859	1,474,416	163.1	1349.3	1172.3
750	248.7	133.8	78,847.6	60,211.5	1,300,108	1,486,621	168.4	1348.3	1159.7
800	257.3	132.7	85,539.6	66,903.5	1,293,451	1,499,272	173.6	1347.6	1147.2
850	265.3	132.4	92,195.6	73,559.5	1,286,827	1,512,339	178.8	1347.1	1134.6
900	272.9	132.5	98,862.0	80,225.9	1,280,207	1,525,796	183.7	1346.8	1122.2
950	280.0	132.8	105,557	86,921.2	1,273,576	1,539,620	188.6	1346.7	1109.7
1000	286.9	133.3	112,273	93,636.7	1,266,924	1,553,794	193.2	1346.8	1097.2

Table 10
Thermodynamic data for TbFeO₃(s)

T/K	S_T^o/ $\mathrm{J\,K^{-1}\,mol^{-1}}$	$C_{p,m}^o$/ $\mathrm{J\,K^{-1}\,mol^{-1}}$	$H_T^o-H_0^o$/ $\mathrm{J\,mol^{-1}}$	$H_T^o-H_{298.15}^o$/ $\mathrm{J\,mol^{-1}}$	$-H_T^o$/ $\mathrm{J\,mol^{-1}}$	$-G_T^o$/ $\mathrm{J\,mol^{-1}}$	$-(G_T^o-H_{298.15}^o)/T$/ $\mathrm{J\,K^{-1}\,mol^{-1}}$	$-\Delta_f H_m^o$/ $\mathrm{kJ\,mol^{-1}}$	$-\Delta_f G_m^o$/ $\mathrm{kJ\,mol^{-1}}$
0	0	0							
25	7.793	3.171	41.4150						
50	13.66	16.65	272.834						
75	23.41	32.38	886.836						
100	34.80	47.32	1885.70						
150	58.94	72.40	4905.43						
200	82.31	89.67	8987.01						
250	103.7	101.6	13,787.2						
298.15	122.4	109.499	18,912.4	0	1,372,400	1,408,894	122.4	1372.4	1287.2
300	123.1	109.8	19,114.1	201.7	1,372,197	1,409,121	122.4	1372.3	1286.7
325	131.9	112.9	21,888.5	2976.1	1,369,412	1,412,310	122.8	1372.0	1279.5
350	140.5	115.8	24,741.6	5829.2	1,366,553	1,415,717	123.8	1371.7	1272.4
400	156.3	120.9	30,643.9	11,731.5	1,360,635	1,423,141	126.9	1370.7	1258.3
450	170.8	125.9	36,774.6	17,862.2	1,354,467	1,431,322	131.1	1369.7	1244.3
500	184.3	131.4	43,141.3	24,228.9	1,348,039	1,440,203	135.8	1368.4	1230.5
550	197.1	138.2	49,805.1	30,892.7	1,341,309	1,449,743	140.9	1366.9	1216.7
600	209.6	147.6	56,881.2	37,968.8	1,334,179	1,459,911	146.3	1365.2	1203.2
650	221.9	162.7	64,538.5	45,626.1	1,326,454	1,470,697	151.7	1363.1	1189.7
652	222.4	163.5	64,859.9	45,947.5	1,326,128	1,471,141	151.9	1363.0	1189.2
652	222.4	163.5	64,859.9	45,947.5	1,326,128	1,471,141	151.9	1363.0	1189.2
700	231.9	130.8	71,218.4	52,306.0	1,319,707	1,482,050	157.2	1362.1	1176.5
750	240.8	127.8	77,700.5	58,788.1	1,313,253	1,493,872	162.4	1361.5	1163.2
800	249.0	126.3	84,070.1	65,157.7	1,306,906	1,506,121	167.6	1361.2	1150.0
850	256.6	125.5	90,359.2	71,446.8	1,300,614	1,518,765	172.6	1361.1	1136.8
900	263.8	125.0	96,600.0	77,687.6	1,294,354	1,531,778	177.5	1361.3	1123.6
950	270.6	124.7	102,825	83,912.2	1,288,111	1,545,138	182.2	1361.7	1110.4
1000	276.9	124.6	109,065	90,152.7	1,281,878	1,558,827	186.8	1362.4	1097.2

Table 11
Thermodynamic data for DyFeO₃(s)

T/K	S_T^o/ $\mathrm{J\,K^{-1}\,mol^{-1}}$	$C_{p,m}^o$/ $\mathrm{J\,K^{-1}\,mol^{-1}}$	$H_T^o-H_0^o$/ $\mathrm{J\,mol^{-1}}$	$H_T^o-H_{298.15}^o$/ $\mathrm{J\,mol^{-1}}$	$-H_T^o$/ $\mathrm{J\,mol^{-1}}$	$-G_T^o$/ $\mathrm{J\,mol^{-1}}$	$-(G_T^o-H_{298.15}^o)/T$/ $\mathrm{J\,K^{-1}\,mol^{-1}}$	$-\Delta_f H_m^o$/ $\mathrm{kJ\,mol^{-1}}$	$-\Delta_f G_m^o$/ $\mathrm{kJ\,mol^{-1}}$
0	0	0	0						
25	6.027	3.604	40.6490						
50	12.33	16.06	287.301						
75	21.86	31.91	888.204						
100	33.12	46.96	1876.10						
150	57.36	73.38	4908.99						
200	81.31	92.67	9094.72						
250	103.4	105.1	14,063.1						
298.15	122.4	109.5	19,521.1	0	1,369,400	1,405,893	122.4	1369.4	1283.7
300	123.1	109.8	19,723.7	202.6	1,369,197	1,406,120	122.4	1369.3	1283.2
325	132.0	113.3	22,509.7	2988.6	1,366,407	1,409,310	122.8	1369.0	1276.0
350	140.5	116.6	25,386.0	5864.9	1,363,532	1,412,717	123.8	1368.6	1268.9
400	156.5	122.6	31,369.3	11,848.2	1,357,553	1,420,148	126.9	1367.6	1254.7
450	171.3	128.6	37,630.9	18,109.8	1,351,275	1,428,347	131.0	1366.4	1240.7
500	185.2	135.4	44,189.3	24,668.2	1,344,680	1,437,261	135.8	1364.9	1226.7
550	198.4	143.7	51,123.0	31,601.9	1,337,711	1,446,853	140.9	1363.2	1213.0
600	211.4	155.3	58,572.0	39,050.9	1,330,254	1,457,099	146.3	1361.1	1199.5
647	223.7	172.3	66,221.7	46,700.6	1,322,586	1,467,323	151.5	1358.6	1186.9
647	223.7	172.3	66,221.7	46,700.6	1,322,586	1,467,323	151.5	1358.6	1186.9
650	224.4	143.2	66,644.8	47,123.7	1,322,155	1,467,995	151.9	1358.5	1186.1
700	234.7	136.1	73,523.5	54,002.4	1,315,206	1,479,477	157.5	1357.2	1172.9
750	243.9	133.6	80,170.5	60,649.4	1,308,472	1,491,446	163.1	1356.2	1159.8
800	252.6	132.8	86,696.5	67,175.4	1,301,815	1,503,861	168.6	1355.4	1146.7
850	260.6	132.6	93,179.3	73,658.2	1,295,183	1,516,692	173.9	1354.9	1133.7
900	268.2	132.8	99,663.8	80,142.7	1,288,550	1,529,914	179.1	1354.4	1120.7
950	275.4	133.2	106,162	86,640.8	1,281,902	1,543,504	184.2	1354.3	1107.7
1000	282.2	133.7	112,653	93,131.8	1,275,229	1,557,445	189.1	1354.4	1094.7

Table 12
Thermodynamic data for HoFeO$_3$(s)

T/K	S_T°/ J K^{-1} mol^{-1}	$C_{p,m}^\circ$/ J K^{-1} mol^{-1}	$H_T^\circ - H_0^\circ$/ J mol^{-1}	$H_T^\circ - H_{298.15}^\circ$/ J mol^{-1}	$-H_T^\circ$/ J mol^{-1}	$-G_T^\circ$/ J mol^{-1}	$-(G_T^\circ - H_{298.15}^\circ)/T$/ J K^{-1} mol^{-1}	$-\Delta_f H_m^\circ$/ kJ mol^{-1}	$-\Delta_f G_m^\circ$/ kJ mol^{-1}
0	0	0	0						
25	6.789	6.520	69.4050						
50	16.20	22.77	432.690						
75	28.08	36.51	1176.45						
100	40.27	48.44	2242.51						
150	63.96	70.04	5200.44						
200	86.68	87.59	9169.31						
250	107.6	99.22	13,861.2						
298.15	125.7	109.0	18,822.1	0	1,364,200	1,401,677	125.7	1364.2	1279.5
300	126.3	109.3	19,024.5	202.4	1,363,998	1,401,910	125.7	1364.1	1278.9
325	135.3	112.6	21,808.2	2986.1	1,361,223	1,405,182	126.1	1363.8	1271.8
350	143.7	115.6	24,676.0	5853.9	1,358,369	1,408,670	126.9	1363.4	1264.8
400	159.5	121.1	30,628.6	11,806.5	1,352,449	1,416,256	130.0	1362.4	1250.8
450	174.1	126.5	36,845.9	18,023.8	1,346,262	1,424,601	134.0	1361.3	1236.9
500	187.7	132.5	43,344.7	24,522.6	1,339,792	1,433,649	138.7	1359.9	1223.1
550	200.7	140.1	50,195.4	31,373.3	1,332,987	1,443,362	143.6	1358.4	1209.5
600	213.3	150.8	57,521.8	38,699.7	1,325,734	1,453,712	148.8	1356.5	1196.1
644	224.4	165.7	64,502.1	45,680.0	1,318,796	1,463,341	153.5	1354.4	1184.4
644	224.4	165.7	64,502.1	45,680.0	1,318,796	1,463,341	153.5	1354.4	1184.4
650	225.7	137.3	65,315.1	46,493.0	1,317,968	1,464,692	154.2	1354.2	1182.7
700	235.6	130.3	71,977.7	53,155.6	1,311,309	1,476,230	159.7	1353.2	1169.6
750	244.5	127.5	78,468.3	59,646.2	1,304,871	1,488,236	164.9	1352.5	1156.6
800	252.7	126.1	84,827.8	66,005.7	1,298,534	1,500,667	170.2	1352.0	1143.5
850	260.3	125.3	91,097.2	72,275.1	1,292,250	1,513,493	175.3	1351.8	1130.5
900	267.4	124.9	97,317.5	78,495.4	1,285,996	1,526,688	180.2	1351.7	1117.5
950	274.2	124.7	103,529	84,707.6	1,279,758	1,540,230	185.0	1351.9	1104.4
1000	280.6	124.5	109,775	90,952.6	1,273,528	1,554,100	189.6	1352.5	1091.4

Table 13
Thermodynamic data for ErFeO$_3$(s)

T/K	S_T°/ J K^{-1} mol^{-1}	$C_{p,m}^\circ$/ J K^{-1} mol^{-1}	$H_T^\circ - H_0^\circ$/ J mol^{-1}	$H_T^\circ - H_{298.15}^\circ$/ J mol^{-1}	$-H_T^\circ$/ J mol^{-1}	$-G_T^\circ$/ J mol^{-1}	$-(G_T^\circ - H_{298.15}^\circ)/T$/ J K^{-1} mol^{-1}	$-\Delta_f H_m^\circ$/ kJ mol^{-1}	$-\Delta_f G_m^\circ$/ kJ mol^{-1}
0	0	0	0						
25	9.262	7.757	85.7410						
50	18.78	21.21	448.534						
75	29.85	34.19	1142.01						
100	41.42	46.73	2154.60						
150	64.91	70.37	5091.89						
200	87.73	87.95	9079.50						
250	108.7	100.0	13,795.1						
298.15	127.2	109.8	18,839.5	0	1,400,500	1,438,424	127.2	1400.5	1316.8
300	127.9	110.1	19,042.4	202.9	1,400,296	1,438,660	127.2	1400.4	1316.2
325	136.8	113.6	21,837.6	2998.1	1,397,499	1,441,970	127.6	1400.1	1309.2
350	145.4	116.8	24,720.7	5881.2	1,397,618	1,445,499	128.6	1399.7	1302.3
400	161.4	122.8	30,715.7	11,876.2	1,388,626	1,453,173	131.7	1398.7	1288.4
450	176.2	128.9	36,993.4	18,153.9	1,382,334	1,461,616	135.8	1397.5	1274.7
500	190.1	135.8	43,578.9	24,739.4	1,375,722	1,470,776	140.6	1396.0	1261.1
550	203.4	144.5	50,557.1	31,717.6	1,368,726	1,480,616	145.8	1394.3	1247.7
600	216.5	156.9	58,072.2	39,232.7	1,361,212	1,491,115	151.1	1392.2	1234.4
634	225.5	169.6	63,590.6	44,751.1	1,355,673	1,498,629	154.9	1390.4	1225.6
634	225.5	169.6	63,590.6	44,751.1	1,355,673	1,498,629	154.9	1390.4	1225.6
650	228.9	139.3	65,821.4	46,981.9	1,353,419	1,502,265	156.7	1389.9	1221.4
700	239.1	134.3	72,638.2	53,798.7	1,346,602	1,513,971	162.2	1388.8	1208.5
750	248.3	132.6	79,298.8	60,459.3	1,339,936	1,526,159	167.7	1387.9	1195.7
800	256.8	132.0	85,884.3	67,044.8	1,333,325	1,538,790	173.0	1387.2	1182.9
850	264.8	132.0	92,452.4	73,612.9	1,326,726	1,551,834	178.6	1386.7	1170.1
900	272.4	132.3	99,037.4	80,197.9	1,320,119	1,565,266	183.3	1386.4	1157.4
950	279.6	132.8	105,650	86,810.9	1,313,493	1,579,066	188.2	1386.3	1144.7
1000	286.4	133.4	112,279	93,439.4	1,306,839	1,593,216	192.9	1386.4	1131.9

Table 14
Thermodynamic data for $Sm_3Fe_5O_{12}(s)$

T/K	$S_T^o/$ $J\,K^{-1}\,mol^{-1}$	$C_{p,m}^o/$ $J\,K^{-1}\,mol^{-1}$	$H_T^o-H_0^o/$ $J\,mol^{-1}$	$H_T^o-H_{298.15}^o/$ $J\,mol^{-1}$	$-H_T^o/$ $J\,mol^{-1}$	$-G_T^o/$ $J\,mol^{-1}$	$-(G_T^o-H_{298.15}^o)/T/$ $J\,K^{-1}\,mol^{-1}$	$-\Delta_f H_m^o/$ $kJ\,mol^{-1}$	$-\Delta_f G_m^o/$ $kJ\,mol^{-1}$
0	0	0	0						
25	17.18	19.21	189.144						
50	43.24	62.38	1190.86						
75	77.73	111.5	3358.62						
100	116.7	161.4	6775.42						
150	198.5	247.7	17,009.1						
200	280.5	324.8	31,347.6						
250	360.6	394.3	49,365.4						
298.15	435.1	450.8	69,759.9	0	4,930,500	5,060,225	435.1	4930.5	4590.6
300	437.9	453.5	70,597.8	837.9	4,929,662	5,061,032	435.1	4930.3	4588.5
325	475.1	475.0	82,217.7	12,457.8	4,918,046	5,072,447	436.7	4928.5	4560.1
350	510.9	492.8	94,329.2	24,569.3	4,905,942	5,084,775	440.7	4926.4	4531.8
400	578.7	521.6	119,748.6	49,988.8	4,880,552	5,112,039	453.7	4921.5	4475.7
450	641.6	545.6	146,465.1	76,705.2	4,853,863	5,142,565	471.1	4916.0	4420.3
500	700.2	569.2	174,352.1	104,592.2	4,826,002	5,176,125	491.0	4909.9	4365.5
550	755.8	598.0	203,548.3	133,788.4	4,796,861	5,212,536	512.5	4903.2	4311.4
567	774.2	610.7	213,837.2	144,077.3	4,786,590	5,225,541	520.0	4900.7	4293.2
567	774.2	610.7	213,837.2	144,077.3	4,786,590	5,225,541	520.0	4900.7	4293.2
600	806.4	567.4	232,567.9	162,808.0	4,767,796	5,251,626	535.0	4897.2	4257.9
650	851.7	566.7	260,879.6	191,119.7	4,739,461	5,293,094	557.7	4892.7	4204.9
700	893.8	568.4	289,182.0	219,422.1	4,711,088	5,336,745	580.3	4888.9	4152.1
750	933.1	570.7	317,541.2	247,781.2	4,682,610	5,382,428	602.7	4885.7	4099.5
800	970.0	573.2	346,001.3	276,241.4	4,654,013	5,430,015	624.7	4883.3	4047.2
850	1004.8	575.6	374,586.0	304,826.1	4,625,295	5,479,394	646.2	4881.6	3995.0
900	1037.8	577.9	403,296.7	333,536.8	4,596,457	5,530,466	667.1	4880.8	3942.9
950	1069.1	580.1	432,113.8	362,353.8	4,567,507	5,583,145	687.7	4881.0	3890.8
1000	1098.9	582.2	460,996.1	391,236.1	4,538,448	5,637,350	707.7	4882.5	3838.7

Table 15
Thermodynamic data for $Eu_3Fe_5O_{12}(s)$

T/K	$S_T^o/$ $J\,K^{-1}\,mol^{-1}$	$C_{p,m}^o/$ $J\,K^{-1}\,mol^{-1}$	$H_T^o-H_0^o/$ $J\,mol^{-1}$	$H_T^o-H_{298.15}^o/$ $J\,mol^{-1}$	$-H_T^o/$ $J\,mol^{-1}$	$-G_T^o/$ $J\,mol^{-1}$	$-(G_T^o-H_{298.15}^o)/T/$ $J\,K^{-1}\,mol^{-1}$	$-\Delta_f H_m^o/$ $kJ\,mol^{-1}$	$-\Delta_f G_m^o/$ $kJ\,mol^{-1}$
0	–	–	–						
25	–	–	–						
50	–	–	–						
75	–	–	–						
100	–	–	–						
150	–	–	–						
200	–	–	–						
250	–	–	–						
298.15	432.2	467.6	–	0	4,650,500	4,779,360	432.2	4650.5	4302.3
300	435.1	469.5	–	867.5	4,649,633	4,780,162	432.2	4650.3	4300.1
325	473.6	492.4	–	12,904.9	4,637,598	4,791,524	433.9	4647.9	4271.0
350	510.8	511.1	–	25,459.6	4,625,047	4,803,832	438.0	4645.1	4242.1
400	581.0	540.0	–	51,802.4	4,598,732	4,831,152	451.5	4638.6	4185.0
450	646.0	562.8	–	79,424.7	4,571,144	4,861,849	469.5	4631.1	4128.8
500	706.3	583.9	–	108,122.6	4,542,477	4,895,676	490.1	4623.1	4073.4
550	763.1	608.8	–	137,959.4	4,512,690	4,932,428	512.3	4614.3	4018.9
559	773.1	614.3	–	143,472.3	4,507,186	4,939,341	516.4	4612.7	4009.1
559	773.1	614.3	–	143,472.3	4,507,186	4,939,341	516.4	4612.7	4009.1
600	814.3	582.3	–	167,369.0	4,483,260	4,971,895	535.4	4606.4	3965.1
650	861.0	582.7	–	196,514.8	4,454,142	5,013,796	558.6	4599.3	3911.9
700	904.2	584.2	–	225,694.2	4,424,969	5,057,940	581.8	4592.6	3859.3
750	944.6	585.7	–	254,929.4	4,395,722	5,104,172	604.6	4586.5	3807.1
800	982.4	587.0	–	284,232.4	4,366,404	5,152,358	627.1	4580.9	3755.4
850	1018.0	588.1	–	313,605.4	4,337,026	5,202,379	649.1	4576.0	3703.9
900	1051.7	588.9	–	343,040.4	4,307,599	5,254,131	670.5	4571.8	3652.7
950	1083.5	589.6	–	372,519.4	4,278,133	5,307,520	691.4	4568.6	3601.8
1000	1113.8	590.2	–	402,014.4	4,248,637	5,362,461	711.8	4566.5	3550.9

Table 16
Thermodynamic data for $Gd_3Fe_5O_{12}(s)$

T/K	$S_T^o/$ $J\,K^{-1}\,mol^{-1}$	$C_{p,m}^o/$ $J\,K^{-1}\,mol^{-1}$	$H_T^o-H_0^o/$ $J\,mol^{-1}$	$H_T^o-H_{298.15}^o/$ $J\,mol^{-1}$	$-H_T^o/$ $J\,mol^{-1}$	$-G_T^o/$ $J\,mol^{-1}$	$-(G_T^o-H_{298.15}^o)/T/$ $J\,K^{-1}\,mol^{-1}$	$-\Delta_f H_m^o/$ $kJ\,mol^{-1}$	$-\Delta_f G_m^o/$ $kJ\,mol^{-1}$
0	0	0	0						
25	17.93	36.41	227.955						
50	58.39	84.31	1755.85						
75	100.5	125.8	4390.90						
100	142.2	165.4	8039.62						
150	223.9	241.8	18,243.2						
200	303.3	312.4	32,129.2						
250	380.0	375.6	49,366.6						
298.15	450.8	433.0	68,755.2	0	4,902,500	5,036,906	450.8	4902.5	4568.7
300	453.4	434.7	69,557.5	802.2	4,901,697	5,037,742	450.8	4902.4	4566.5
325	489.1	455.2	80,679.9	11,924.7	4,890,563	5,049,527	452.4	4901.5	4538.6
350	523.4	472.0	92,265.6	23,510.3	4,878,965	5,062,187	456.3	4899.9	4510.7
400	588.3	498.3	116,541.9	47,786.6	4,854,673	5,090,004	468.8	4895.6	4455.4
450	648.2	519.4	141,975.5	73,220.2	4,829,214	5,120,939	485.5	4890.3	4400.7
500	704.0	539.6	168,408.5	99,653.2	4,802,741	5,154,762	504.7	4884.5	4346.6
550	756.5	564.2	195,936.7	127,181.0	4,775,179	5,191,289	525.3	4878.1	4293.1
556	762.7	567.9	199,327.1	130,571.9	4,771,783	5,195,846	527.8	4877.3	4286.8
556	762.7	567.9	199,327.1	130,571.9	4,771,783	5,195,846	527.8	4877.3	4286.8
600	803.5	535.4	222,912.0	154,156.7	4,748,162	5,230,317	546.6	4872.8	4240.2
650	846.4	535.6	249,703.6	180,948.3	4,721,395	5,271,582	568.0	4868.3	4187.7
700	886.1	536.7	276,517.0	207,761.7	4,694,588	5,314,910	589.3	4864.3	4135.5
750	923.2	538.0	303,375.6	234,620.3	4,667,718	5,360,156	610.4	4860.9	4083.5
800	958.0	539.2	330,293.3	261,538.0	4,640,787	5,407,196	631.0	4858.2	4031.8
850	990.7	540.2	357,274.0	288,518.7	4,613,801	5,455,923	651.2	4856.1	3980.2
900	1021.6	541.0	384,311.8	315,556.6	4,586,770	5,506,239	671.0	4854.9	3928.7
950	1050.9	541.7	411,391.1	342,635.9	4,559,703	5,558,059	690.2	4854.7	3877.3
1000	1078.6	542.1	438,486.5	369,731.2	4,532,606	5,611,305	708.9	4855.7	3825.8

Table 17
Thermodynamic data for $Tb_3Fe_5O_{12}(s)$

T/K	$S_T^o/$ $J\,K^{-1}\,mol^{-1}$	$C_{p,m}^o/$ $J\,K^{-1}\,mol^{-1}$	$H_T^o-H_0^o/$ $J\,mol^{-1}$	$H_T^o-H_{298.15}^o/$ $J\,mol^{-1}$	$-H_T^o/$ $J\,mol^{-1}$	$-G_T^o/$ $J\,mol^{-1}$	$-(G_T^o-H_{298.15}^o)/T/$ $J\,K^{-1}\,mol^{-1}$	$-\Delta_f H_m^o/$ $kJ\,mol^{-1}$	$-\Delta_f G_m^o/$ $kJ\,mol^{-1}$
0	0	0	0						
25	17.71	29.76	227.920						
50	52.23	74.70	1537.45						
75	90.75	117.8	3948.66						
100	130.3	153.9	7417.34						
150	212.9	254.2	17,765.6						
200	296.4	326.1	32,366.8						
250	375.4	381.7	50,110.6						
298.15	446.9	432.2	69,702.3	0	4,942,500	5,075,743	446.9	4942.5	4602.7
300	449.5	434.0	70,504.0	801.7	4,941,698	5,076,572	446.9	4942.4	4600.6
325	485.2	455.8	81,636.2	11,933.9	4,930,564	5,088,259	448.4	4941.0	4572.1
350	519.6	473.7	93,261.9	23,559.6	4,918,938	5,100,823	452.3	4939.2	4543.8
400	584.8	501.9	117,699.5	47,997.2	4,894,514	5,128,457	464.8	4934.6	4487.6
450	645.3	524.6	143,390.3	73,688.0	4,868,836	5,159,230	481.5	4929.3	4432.1
500	701.7	546.2	170,166.4	100,464.1	4,842,067	5,192,921	500.7	4923.2	4377.2
550	754.9	572.2	198,118.3	128,416.0	4,814,138	5,229,347	521.4	4916.5	4322.9
556	761.1	576.1	201,565.4	131,863.1	4,810,693	5,233,896	523.9	4915.6	4316.4
556	761.1	576.1	201,565.4	131,863.1	4,810,693	5,233,896	523.9	4915.6	4316.4
600	802.7	544.7	225,535.7	155,833.4	4,786,687	5,268,313	542.9	4910.8	4269.2
650	846.3	546.1	252,824.8	183,122.5	4,759,423	5,309,554	564.6	4906.0	4215.9
700	886.9	548.5	280,197.6	210,495.3	4,732,056	5,352,897	586.2	4901.6	4163.0
750	924.8	551.0	307,676.1	237,973.8	4,704,567	5,398,201	607.5	4897.9	4110.4
800	960.4	553.3	335,272.9	265,570.6	4,676,956	5,445,344	628.5	4893.4	4058.0
850	994.0	555.5	362,990.8	293,288.5	4,649,234	5,494,216	649.0	4892.3	4005.8
900	1025.9	557.4	390,823.5	321,121.2	4,621,408	5,544,723	669.1	4890.6	3953.7
950	1056.0	559.2	418,754.6	349,052.3	4,593,489	5,596,780	688.6	4890.0	3901.6
1000	1084.8	560.9	446,758.5	377,056.2	4,565,484	5,650,308	707.7	4890.6	3849.6

Table 18
Thermodynamic data for Dy$_3$Fe$_5$O$_{12}$(s)

T/K	S°_T/ J K^{-1} mol^{-1}	$C^\circ_{p,m}$/ J K^{-1} mol^{-1}	$H^\circ_T - H^\circ_0$/ J mol^{-1}	$H^\circ_T - H^\circ_{298.15}$/ J mol^{-1}	$-H^\circ_T$/ J mol^{-1}	$-G^\circ_T$/ J mol^{-1}	$-(G^\circ_T - H^\circ_{298.15})/T$/ J K^{-1} mol^{-1}	$-\Delta_f H^\circ_m$/ kJ mol^{-1}	$-\Delta_f G^\circ_m$/ kJ mol^{-1}
0	0	0	0						
25	22.72	24.85	276.812						
50	47.77	54.69	1220.89						
75	79.57	108.2	3226.83						
100	118.5	166.6	6648.71						
150	200.9	243.5	16,935.8						
200	280.6	312.6	30,875.3						
250	357.1	373.4	48,063.8						
298.15	427.3	426.2	67,285.9	0	4,895,500	5,022,899	427.3	4895.5	4548.4
300	429.9	427.6	68,076.0	790.1	4,894,710	5,023,692	427.3	4895.4	4546.2
325	464.8	445.4	78,998.5	11,712.6	4,883,788	5,034,880	428.8	4894.1	4517.2
350	498.4	460.1	90,326.5	23,040.6	4,872,464	5,046,925	432.6	4892.6	4488.3
400	561.5	483.9	113,968.8	46,682.9	4,848,838	5,073,447	444.8	4888.8	4430.8
450	619.6	503.9	138,684.8	71,398.9	4,824,134	5,102,996	461.0	4884.3	4373.8
500	673.8	523.8	164,384.4	97,098.3	4,798,447	5,135,348	479.6	4879.3	4317.3
550	724.8	549.1	191,204.1	123,918.2	4,771,659	5,170,325	499.5	4873.6	4261.4
554	728.8	551.6	193,407.5	126,121.6	4,769,457	5,173,232	501.1	4873.1	4256.9
554	728.8	551.6	193,407.5	126,121.6	4,769,457	5,173,232	501.1	4873.1	4256.9
600	770.3	519.7	217,323.4	150,037.6	4,745,500	5,207,728	520.3	4869.1	4205.9
650	812.0	520.8	243,352.3	176,066.4	4,719,495	5,247,301	541.1	4865.2	4150.9
700	850.6	523.0	269,454.0	202,168.1	4,693,400	5,288,880	561.8	4861.8	4096.0
750	886.8	525.5	295,657.6	228,371.7	4,667,186	5,332,328	582.3	4858.9	4041.4
800	920.8	527.9	321,981.8	254,695.9	4,640,849	5,377,529	602.4	4856.6	3987.0
850	952.9	530.3	348,434.7	281,148.8	4,614,391	5,424,381	622.1	4854.9	3932.7
900	983.3	532.5	375,014.1	307,728.2	4,587,819	5,472,794	641.3	4853.9	3878.5
950	1012.1	534.6	401,707.5	334,421.6	4,561,138	5,522,686	660.1	4853.9	3824.3
1000	1039.6	536.7	428,491.8	361,205.9	4,534,352	5,573,986	678.4	4855.1	3770.1

Table 19
Thermodynamic data for Ho$_3$Fe$_5$O$_{12}$(s)

T/K	S°_T/ J K^{-1} mol^{-1}	$C^\circ_{p,m}$/ J K^{-1} mol^{-1}	$H^\circ_T - H^\circ_0$/ J mol^{-1}	$H^\circ_T - H^\circ_{298.15}$/ J mol^{-1}	$-H^\circ_T$/ J mol^{-1}	$-G^\circ_T$/ J mol^{-1}	$-(G^\circ_T - H^\circ_{298.15})/T$/ J K^{-1} mol^{-1}	$-\Delta_f H^\circ_m$/ kJ mol^{-1}	$-\Delta_f G^\circ_m$/ kJ mol^{-1}
0	0	0	0						
25	47.42	34.85	336.205						
50	84.57	76.81	1736.26						
75	123.4	117.7	4169.64						
100	162.8	156.4	7613.76						
150	242.6	241.5	17,601.7						
200	322.7	317.1	31,608.2						
250	400.8	383.3	49,160.4						
298.15	473.1	445.7	68,973.7	0	4,925,600	5,066,654	473.1	4925.6	4592.1
300	475.8	447.4	69,799.6	825.9	4,924,773	5,067,532	473.1	4925.4	4590.0
325	512.4	467.4	81,236.1	12,262.3	4,913,328	5,079,889	474.7	4923.6	4562.1
350	547.7	483.9	93,126.3	24,152.5	4,901,429	5,093,146	478.7	4921.4	4534.4
400	614.1	510.0	117,993.7	49,020.0	4,876,550	5,122,216	491.6	4916.3	4479.4
450	675.4	531.4	144,018.4	75,044.7	4,850,503	5,154,477	508.7	4910.5	4425.1
500	732.5	552.6	171,080.7	102,107.0	4,823,410	5,189,695	528.3	4904.0	4371.6
546	782.2	577.3	197,013.7	128,040.0	4,797,454	5,224,543	547.7	4897.5	4322.9
546	782.2	577.3	197,013.7	128,040.0	4,797,454	5,224,543	547.7	4897.5	4322.9
550	786.2	548.2	199,201.4	130,227.6	4,795,259	5,227,680	549.4	4897.0	4318.6
600	833.7	545.1	226,519.7	157,545.9	4,767,961	5,268,197	571.1	4891.3	4266.3
650	877.3	546.0	253,826.6	184,852.8	4,740,687	5,310,989	592.9	4886.2	4214.4
700	917.9	547.7	281,167.6	212,193.9	4,713,343	5,355,884	614.7	4881.5	4163.0
750	955.7	549.4	308,575.0	239,601.2	4,685,912	5,402,736	636.3	4877.3	4111.8
800	991.2	551.0	336,067.4	267,093.6	4,658,400	5,451,421	657.4	4873.7	4060.9
850	1024.7	552.3	363,650.1	294,676.4	4,630,814	5,501,830	678.0	4870.8	4010.2
900	1056.3	553.5	391,315.1	322,341.4	4,603,164	5,553,863	698.1	4868.8	3959.6
950	1086.2	554.6	419,040.9	350,067.2	4,575,457	5,607,435	717.8	4867.7	3909.1
1000	1114.7	555.5	446,792.7	377,818.9	4,547,702	5,662,468	736.9	4868.0	3858.7

Table 20
Thermodynamic data for $Er_3Fe_5O_{12}(s)$

T/K	$S_T^\circ/$ $J\,K^{-1}\,mol^{-1}$	$C_{p,m}^\circ/$ $J\,K^{-1}\,mol^{-1}$	$H_T^\circ-H_0^\circ/$ $J\,mol^{-1}$	$H_T^\circ-H_{298.15}^\circ/$ $J\,mol^{-1}$	$-H_T^\circ/$ $J\,mol^{-1}$	$-G_T^\circ/$ $J\,mol^{-1}$	$-(G_T^\circ-H_{298.15}^\circ)/T/$ $J\,K^{-1}\,mol^{-1}$	$-\Delta_f H_m^\circ/$ $kJ\,mol^{-1}$	$-\Delta_f G_m^\circ/$ $kJ\,mol^{-1}$
0	0	0	0						
25	36.90	35.01	434.878						
50	70.81	69.04	1708.18						
75	105.6	105.2	3886.62						
100	141.0	142.8	6982.72						
150	214.9	232.0	16,245.7						
200	292.7	309.7	29,865.1						
250	368.9	373.3	46,988.3						
298.15	483.9	428.0	66,294.6	0	5,023,500	5,167,774	483.9	5023.5	4694.8
300	486.6	432.1	67,092.3	797.6	5,022,702	5,168,672	483.9	5023.4	4692.8
325	521.9	452.2	78,147.7	11,853.0	5,011,640	5,181,281	485.5	5022.0	4665.3
350	556.1	468.8	89,660.2	23,365.6	5,000,122	5,194,760	489.3	5020.2	4637.9
400	620.5	495.3	113,786.3	47,491.6	4,975,992	5,224,197	501.7	5016.0	4583.6
450	680.1	517.3	139,095.8	72,801.2	4,950,668	5,256,732	518.3	5010.9	4529.8
500	735.8	539.2	165,479.0	99,184.3	4,924,266	5,292,144	537.3	5005.3	4476.6
544	782.2	563.6	189,701.4	123,406.7	4,900,034	5,325,546	555.3	4999.7	4430.4
544	782.2	563.6	189,701.4	123,406.7	4,900,034	5,325,546	555.3	4999.7	4430.4
550	788.0	534.2	192,899.2	126,604.6	4,896,825	5,330,256	557.8	4999.1	4424.1
600	834.4	532.1	219,543.1	153,248.4	4,870,200	5,370,835	578.9	4994.2	4372.0
650	877.0	533.7	246,214.9	179,920.3	4,843,559	5,413,634	600.2	4989.8	4320.4
700	916.7	536.1	272,957.2	206,662.6	4,816,813	5,458,489	621.4	4985.9	4269.0
750	953.7	538.4	299,799.6	233,504.9	4,789,949	5,505,260	642.4	4982.4	4218.0
800	988.6	540.7	326,759.2	260,464.6	4,762,970	5,553,826	662.9	4979.6	4167.1
850	1021.4	542.7	353,840.7	287,546.1	4,735,885	5,604,084	683.1	4977.4	4116.4
900	1052.5	544.6	381,036.0	314,741.4	4,708,704	5,655,938	702.8	4975.9	4065.8
950	1081.9	546.3	408,324.6	342,029.9	4,681,433	5,709,306	721.9	4975.4	4015.2
1000	1110.0	547.8	435,673.1	369,378.5	4,654,081	5,764,111	740.6	4976.2	3964.7

heat capacity anomaly for the rare-earth iron garnets $R_3Fe_5O_{12}(s)$ observed in the temperature range 540–560 K are assigned due to magnetic order–disorder transformation from ferrimagnetic to paramagnetic state. It has been observed that for the garnets the transition temperature (Curie temperature, T_C) is nearly invariant for different R.

Thermodynamic tables are generated for some of the orthoferrites and garnet compounds by coupling the heat capacity data obtained in the present study with the very low temperate data from the literature. These tables are useful for any type of thermochemical calculations where the above-mentioned compounds are used.

Appendix A. Supplementary Materials

Supplementary data associated with this article can be found in the online version at doi:10.1016/j.jssc.2007.11.003.

References

[1] C.P. Khattak, F.F.Y. Wang, in: K.A. Gschneidner Jr., L. Eyring (Eds.), Handbook of the Physics and Chemistry of Rare Earths, North-Holland, Amsterdam, 1979, pp. 525–607.
[2] K. Ueda, H. Tabata, T. Kawai, Science 280 (1998) 1064–1066.
[3] K. Ueda, H. Tabata, T. Kawai, Phys. Rev. B 60 (1999) R12561–R12564.
[4] F. Sayetat, J. Magn. Magn. Mater. 58 (1986) 334–346.
[5] M. Marezio, P.D. Dernier, Mater. Res. Bull. 6 (1971) 23–30.
[6] J. Blasco, J. Garcia, J. Phys. Chem. Solids 55 (1994) 843.
[7] D.J. Lam, B.W. Veal, D.E. Ellis, Phys. Rev. B 22 (1980) 5730.
[8] R.G. Burns, in: A. Navrotsky, D.J. Weidner (Eds.), Geophysical Monograph 45, Perovskite: A Structure of Great Interest to Geophysics and Materials Science, American Geophysical Union, Washington, DC, 1981, p. 81.
[9] H. Horner, C.M. Varma, Phys. Rev. Lett. 20 (1968) 845.
[10] W.C. Koehler, E.O. Wollan, M.K. Wilkinson, Phys. Rev. 118 (1960) 58.
[11] F. Bartolome, M.D. Kuz'min, J. Bartolome, J. Blasco, J. Garcia, F. Sapina, Solid-State Commun. 91 (1994) 177–182.
[12] A. de Combarieu, J. Mareschal, J.C. Michel, J. Sivardiere, Solid-State Commun. 6 (1968) 257–259.
[13] K.P. Belov, A.M. Kadomtseva, L.M. Leneva, T.L. Orchinnikova, Ya.G. Panomarev, V.A. Timofeeva, Sov. Phys. Solid State 9 (1968) 2190.
[14] G. Gorodetsky, B. Sharon, S. Shtrikman, Solid State Commun. 5 (1968) 739.
[15] G. Gorodetsky, B. Sharon, S. Shtrikman, J. Appl. Phys. 39 (1968) 1371.
[16] A. Berton, B. Sharon, J. Appl. Phys. 39 (1968) 1367–1368.
[17] M.R. Moldover, G. Sjolander, W. Weyhmann, Phys. Rev. Lett. 26 (1971) 1257–1259.
[18] A. Bhattacharjee, K. Saito, M. Sorai, J. Phys. Chem. Solids 63 (2002) 569–574.
[19] K. Saito, Y. Yamamura, J. Mayer, H. Kobayashi, Y. Miyazaki, J. Ensling, P. Gutlich, B. Lesniewska, M. Sorai, J. Magn. Magn. Mater. 225 (2001) 381–388.
[20] M. Eibschutz, S. Shtrikman, D. Treves, Phys. Rev. 156 (1967) 562.
[21] S. Stølen, F. Grønvold, H. Brinks, T. Atake, H. Mori, J. Chem. Thermodyn. 30 (1998) 365–377.
[22] W.P. Wolf, R.L. White, J. Appl. Phys. 40 (1969) 1061–1069.

[23] S. Geller, M.A. Gilleo, J. Phys. Chem. Solids 3 (1957) 30.
[24] F. Bertaut, F. Forrat, A. Herpin, P. Meriel, C.R. Acad. Sci. Paris 243 (1956) 898.
[25] R. Pauthenet, Ann. Phys. 3 (1958) 424–462.
[26] R. Pauthenet, J. Appl. Phys. 30 (1959) 290S–292S.
[27] R. Pauthenet, J. Phys. Radium 20 (1959) 388.
[28] Aleonard, J. Phys. Chem. Solids 15 (1960) 167.
[29] B.H. Justice, E.F. Westrum Jr., J. Phys. Chem. 67 (1963) 339–345.
[30] B.H. Justice, E.F. Westrum Jr., J. Phys. Chem. 67 (1963) 345–351.
[31] B.H. Justice, E.F. Westrum Jr., J. Phys. Chem. 67 (1963) 659–665.
[32] F. Gronvold, E.J. Samuelsen, J. Phys. Chem. Solids 36 (1975) 249–256.
[33] W. Schnelle, R. Fischer, E. Gmelin, J. Phys. D: Appl. Phys. 34 (2001) 846–851.
[34] S.C. Parida, S. Dash, Z. Singh, R. Prasad, V. Venugopal, J. Solid State Chem. 164 (2002) 34–41.
[35] S.C. Parida, K.T. Jacob, V. Venugopal, J. Phase Equilibria 24 (2003) 431–446.
[36] J.D. Cashion, A.H. Cooke, D.M. Martin, M.R. Wells, J. Phys. C: Solid State Phys. 3 (1970) 1612–1620.
[37] S.C. Parida, K.T. Jacob, V. Venugopal, Solid State Sci. 4 (2002) 1245–1255.
[38] K. Saito, A. Sato, A. Bhattacharjee, M. Sorai, Solid State Commun. 120 (2001) 129–132.
[39] A.B. Harris, H. Meyer, Phys. Rev. 127 (1962) 101–118.
[40] A.J. Henderson Jr., D.G. Onn, H. Meyer, Phys. Rev. 185 (1969) 1218–1229.
[41] V.S. Varazashvili, M.S. Tsarakhov, G.D. Chachanidze, Neorgan. Mater. 26 (1990) 602–604.
[42] T.B. Mirianashvili, V.S. Varazashvili, M.S. Tsarakhov, T.A. Pavlenishvili, Russ. J. Inorg. Chem. 42 (1997) 926–928.
[43] V.S. Varazashvili, M.S. Tsarakhov, T.B. Mirianashvili, Russ. J. Inorg. Chem. 42 (1997) 597–599.
[44] R. Moretti, G. Ottonello, Geochim. Cosmochim. Acta 62 (1998) 1147–1173.